Doctoral Dissertation

博士論文（要約）

# Elucidation of the amplification mechanism of meteo-tsunamis originating west of Kyushu Island and proposal for a possible forecasting system

（九州西方沿岸域で発生する気象津波の増幅機構の解明とその予報システムの提案）

A Dissertation Submitted for the Degree of Doctor of Philosophy

December 2019

令和元年１２月博士（理学）申請

Department of Earth and Planetary Science, Graduate School of Science,

The University of Tokyo

東京大学大学院理学系研究科

地球惑星科学専攻

Katsutoshi Fukuzawa

福澤　克俊

# Abstract

A meteo-tsunami (meteorological tsunami) is a tsunami-like phenomenon excited by a traveling atmospheric disturbance associated with some meteorological phenomena. It has been observed and reported in the world such as the Adriatic Sea, the Black Sea, the Great Lakes, the Mediterranean Sea, and the East China Sea. In Japan, meteo-tsunamis are frequently observed on the western coast of Kyushu Island, in particular, in Nagasaki Bay and Makurazaki Bay. The amplitude of meteo-tsunamis sometimes reaches several meters at certain bays or harbors and causes flooding; they have a large impact on coastal societies. However, their forecasts have not yet been realized in spite of their necessity.

In the last few decades, it has been reported that two resonant processes play a key role in exciting meteo-tsunamis: the resonant coupling between the atmospheric disturbance and generated oceanic waves (Proudman resonance), and resonant amplification by the bay's eigen-oscillations. However, most of the previous studies did not discuss the transient response of a bay in a meteo-tsunami, that is any system supplying continuously oceanic waves to the bay is insufficiently understood. This thesis discusses the amplification mechanism, in particular a system creating oceanic waves, and examines the possibilities of forecasting meteo-tsunamis focusing on the west coast of Kyushu Island.

One of the largest meteo-tsunamis occurred on March 3, 2010, where the maximum amplitude of sea level oscillations exceeded 1 m in various bays on the western coast of Kyushu Island including Nagasaki Bay and Makurazaki Bay. Simultaneously, a sequence of rapid atmospheric pressure changes with amplitudes of ~1 hPa was recorded at various meteorological stations along the western coast of Kyushu Island.

We numerically reproduce large sea level oscillations in both bays assuming that a simple atmospheric pressure disturbance consisting of a sequence of pressure changes in 10-20 min propagates east-southeastward at a speed of ~30 m/s over the East China Sea. Over a wide area of the shallow continental shelf in the East China Sea, oceanic waves

are amplified through a resonant coupling to the traveling atmospheric disturbance. Oceanic waves propagate eastward while being further amplified through reflection and refraction owing to the complicated topographic and configuration constraints in the coastal area and excite meteo-tsunamis along the western coast of Kyushu Island. In particular, the eigen-oscillations are excited on the continental shelf, which continue to supply oceanic waves that are resonant with eigen-oscillations both in Nagasaki Bay and Makurazaki Bay. It is confirmed that the amplification mechanism worked also in other meteo-tsunamis in the winter of 2012 and 2004.

In order to forecast the occurrence of meteo-tsunamis, two approaches are thought to be useful: identifying atmospheric conditions generating meteo-tsunamis and real-time detection of significant atmospheric or oceanic disturbances before the amplitude of sea level oscillations grows in a bay. Because the former approach is mainly based on atmospheric modeling being subject to big uncertainties, the latter approach using oceanic modeling is thought to be more useful. To real-time detect a meteo-tsunami wave originating west of Kyushu Island, a vertical observation network is distributed: sea level instrument arrayed at the westernmost island in Kyushu and airborne radar altimetry attached to commercial airplanes. In this thesis, based on observation of oceanic waves in the East China Sea, we propose a forecasting system which estimates propagation direction and period of oceanic waves and forecasts sea level oscillations in a bay. The performance of this forecasting system is assessed for the case study of the 2010 meteo-tsunami to show that the maximum amplitudes of the meteo-tsunami can be forecasted with an error of about 25%.

Overall, the results in this thesis will serve for the realization of an operational forecasting system of meteo-tsunamis.

# Contents

# Chapter 1

# General Introduction

## 1.1 Meteo-tsunami (meteorological tsunami)

The term “tsunami” originally means a big wave in a bay or harbor whatever its source is. Although the term is frequently used to refer to an oceanic wave generated by seismic movements, it also means an oceanic wave generated by other mechanisms, say, by submarine landslides, volcanic eruptions, or meteorite falls.

There is one more type of sea level oscillations in a specific bay or harbor which should be called “tsunami” but is not related to significant precursory phenomena listed above. Some studies pointed out that it can be caused by atmospheric pressure forcing or wind stress forcing associated with some meteorological phenomena such as atmospheric gravity waves, front lines, squalls, etc.

The “tsunami” events caused by meteorological phenomena were observed and reported at many coastal places in the world (C. B. Pattiaratchi and Wijeratne, 2015; Vilibić et al., 2016) (see Figure 1.1 and Table 1.1): the Mediterranean Sea (Drago, 2009; Ličer et al., 2017; Šepić et al., 2018; Vilibić et al., 2008), the Adriatic Sea (Vilibić et al., 2006; Orlić et al., 2010; Šepić et al., 2012; Šepić et al., 2016), the Black Sea (Vilibić et al., 2010), the Baltic Sea (Pellikka et al., 2015), the Indian Ocean (Indika et al., 2017; Mehra et al., 2012), the North Sea (de Jong and Battjes, 2004), the English Channel (Williams et al., 2019), the Persian Gulf (Heidarzadeh et al., 2019), the Great Lakes (Linares et al., 2016), the Yellow Sea (H. Kim et al., 2017; M.-S. Kim et al., 2019), the East China Sea (Hibiya and Kajiura, 1982; Tanaka, 2010), the coast of Australia (Pattiaratchi and Wijeratne, 2015a; Pattiaratchi and Wijeratne, 2015b), the coast of New Zealand (Goring, 2009), the coast of South Africa (Okal et al., 2014), the coast of North America (Thomson et al., 2009; Pasquet and Vilibić, 2013; Wertman et al., 2014) and South America (Perez and Walter, 2017; Carvajal et al., 2017). At certain places, the sea level oscillations caused by atmospheric forcing have local names: “rissaga” in the Balearic Islands; “marrobbio” in Sicily; “mulghuba” in Malta; “šćiga” in the Adiatic Sea; “seebär” in the Baltic Sea; “abiki” in Japan (Monserrat et al., 2006; Rabinovich, 2019). Nowadays, this phenomenon has a general name, “meteorological tsunami”, “meteotsunami”, or “meteo-tsunami” after the fact that it is associated with meteorological phenomena.

The amplitude of sea level oscillations sometimes reaches several meters at certain bays or harbors and brings about overflow of water and inundation. In addition,

strong current related with the sea level oscillations drags and breaks boats free from the moorings. In fact, the large meteo-tsunami, which occurred in Ciutadella Harbor, Menorca, Spain on June 15, 2006, damaged more than 40 boats and caused an economic loss of several tens millions of euros (Monserrat et al., 2006). In the worst cases, people can be drowned by meteo-tsunamis.

## 1.2 General amplification mechanism of meteo-tsunamis

### 1.2.1 Harbor oscillations

The transient response of a bay or harbor to an incident oceanic wave depends on the seaward radiation of energy from its entrance. After an oceanic wave enters the bay, it is reflected at the bay head, travels toward its entrance, and is re-reflected partially at its entrance. The degree of wave reflection at the entrance of the bay, $R$, is strongly related with the aspect ratio of the bay, $\theta = b/l$, where $b$ is the width of the entrance and $l$ is the width of the basin (Rabinovich, 2009). In a closed (open) bay whose $\theta$ is small (large) and $R$ is large (small), an oceanic wave is hard (easy) to path through the entrance so that sea level oscillations continue for a long (short) time. Consequently, the amplitude of sea level oscillations in a closed bay is amplified when oceanic waves are continuously supplied.

When oceanic waves with a period of $\omega$ continue to be supplied to a bay whose lowest eigen-mode frequency is $\omega_0$, the amplification ratio of amplitude of sea level oscillations is

$$H^2(\omega) = \frac{1}{(1-\frac{\omega}{\omega_0})^2 + \frac{1}{Q^2}(\frac{\omega}{\omega_0})^2} \qquad (1\text{-}1)$$

where $Q$ is the quality factor, a measure of the energy damping of the bay (Miles and Munk, 1961). Note that this formulation can be applied to a bay with a simple shape which is thought to be a system with one degree of freedom like a pendulum. Large value of $Q$ indicates that the amplitude of sea level oscillations keeps growing over a long time when oceanic waves with the resonant frequency continuously come into the bay and decays slowly (e.g. Rabinovich, 2009). The value of $Q$ at the resonant frequency can be estimated as the ratio of the resonant frequency, $\omega_0$, to bandwidth between frequencies, $\omega_{1/2}{}^{\pm}$, at which the power spectral density of sea level variations is half of that at the

resonant frequency,

$$Q = \frac{\omega_0}{\omega_{1/2}^{+} - \omega_{1/2}^{-}}. \quad (1\text{-}2)$$

As for a bay which has a dominant oscillation mode and can be thought to be an oscillatory system with one degree of freedom, the transient response of the bay to an arbitrary series of incident oceanic waves can be described using the value of $Q$ without numerical simulations. Indeed, Endoh et al. (2018) examined the possibility taking the response of Miyako Bay and Kushimoto Bay to the incident seismic tsunami waves as an example, indicating that $Q$ is a factor representing the response of the bay. Note that, in order to reconstruct the transient response in a bay using this method, it is essential to observe incident waves accurately.

### 1.2.2 Amplification mechanism of meteo-tsunamis

The first study of clarifying the amplification mechanism of a meteo-tsunami is Hibiya and Kajiura (1982), who focused on the meteo-tsunami in Nagasaki Bay on March 31, 1979. They numerically showed that two resonance processes played a key role in amplifying the oceanic waves, the Proudman resonance (Proudman, 1929) and the resonant connection between the eigen-oscillations with a larger spatial scale and those with a smaller spatial scale, schematically sketched in Figure 1.2. In the former resonant process, the atmospheric pressure disturbance propagated east-northeastward with a speed of about 30 m/s over the shallow continental shelf in the East China Sea with a depth of about 100 m and coupled with an oceanic gravity wave. In the latter process, one of the eigen-oscillations formed on the continental shelf surrounded by the northwestern coast of Kyushu Island and the Goto Islands (Goto Nada) shared nearly the same period with the first mode oscillation in Nagasaki Bay, so that oceanic waves resonant with the eigen-oscillation in Nagasaki Bay were continuously supplied from Goto Nada.

Motivated by Hibiya and Kajiura (1982), many studies were conducted and explained the amplification mechanism of local meteo-tsunamis at the respective area. The importance of the Proudman resonance and the resonant amplification of the eigen-oscillations was pointed out by a number of papers focusing on most of the areas mentioned above. For instance, meteo-tsunamis in Ciutadella Harbor were generated by the Proudman resonance over the continental shelf surrounding the Balearic Islands and

the resonant amplification of the eigen-oscillations in Ciutadella Harbor (Monserrat et al., 2006). Meteo-tsunamis along the U. S. East Coast were caused by the Proudman resonance over the continental shelf running north-south along the coastline and the reflection of oceanic waves at the eastern shelf break (Pasquet and Vilibić, 2013; Wertman et al., 2014). In addition, the resonant coupling between the propagating atmospheric pressure disturbance and an oceanic edge wave, the Greenspan resonance (Greenspan, 1956), was shown to play an important role in generating meteo-tsunamis in some areas such as the Great Lakes (Bechle and Wu, 2014; Linares et al., 2016) and the English Channel (Williams et al., 2019). The fact that meteo-tsunamis are observed at places near the continental shelf region with a depth about 100 m (see Figure 1.1) implies that the amplification mechanism, Proudman resonance or the Greenspan resonance, is essential for their generation. Motivated by the importance of the Proudman resonance, some numerical studies were conducted focusing on the degree to which an oceanic wave is amplified due to the Proudman resonance for some patterns of the forcing and bathymetry (Bubalo et al., 2018; Vilibić, 2008). Note that atmospheric pressure disturbances are main triggers of meteo-tsunamis and wind stress disturbances are secondary ones except in shallow areas with a depth of the order of 10 m (Shi et al., 2019).

Given the fact that most of the papers on meteo-tsunamis emphasize the essential role of the Proudman resonance and the eigen-oscillations of a bay, it is suggested that the location and the shape of a bay determine whether or not large meteo-tsunamis occur in the bay; they occur in a bay (i) which is located near a large continental shelf over which significant atmospheric disturbances frequently travel and (ii) has a shape with a large value of $Q$. However, are these characteristics sufficient conditions for the occurrence of large meteo-tsunamis? There is a possibility that the existence of an outer system continuously supplying oceanic waves to the bay is also essential as was for the 1979 meteo-tsunami in Nagasaki Bay. The degree to which such a system contributes to the amplification should be examined.

Although many studies have been conducted to numerically simulate a meteo-tsunami, they fail to numerically reconstruct the observed sea level variations and compare the simulated sea level variations with observed ones (e.g. Vilibić et al., 2010) except some studies (e.g. Hibiya and Kajiura, 1982; Vilibić et al., 2006). This indicates

that the amplification mechanism has not yet been clarified enough; whether a system continuously supplying oceanic waves to a bay universally exists near the bay or not has not been discussed. If there is an outer system creating and supplying a series of oceanic waves to the bay, large sea level oscillations are generated in the bay by only small number of atmospheric pressure disturbance waves. It is one of the motivations of this thesis to examine whether the existence of an outer system supplying oceanic waves to a bay is universal amplification mechanism of meteo-tsunamis or not.

## 1.3 The difficulty of forecasting meteo-tsunamis

Since some atmospheric disturbance generates a meteo-tsunami, many studies have been conducted to reconstruct the atmospheric conditions of generating the meteo-tsunami. Although it is essential that an atmospheric disturbance propagates a long distance to cause a meteo-tsunami, two mechanisms which maintain the energy of the atmospheric disturbance are suggested: wave-duct (Monserrat and Thorpe, 1996) and wave-CISK (Belušić et al., 2007). The former mechanism is that an atmospheric pressure disturbance is trapped in the lower troposphere due to wave reflection at the middle height of troposphere (Lindzen and Tung, 1976). On the other hand, the latter one is that the energy is added to the atmospheric disturbance by convection during its propagation (Lindzen, 1974).

Although there exist many discussions on the synoptic atmospheric synoptic conditions suitable to cause meteo-tsunamis (e.g. Šepić et al., 2016b), the observed atmospheric disturbances with high frequencies have not been accurately reconstructed due to the limitations of the atmospheric model such as the uncertainties of initial conditions, spatial and temporal model resolution and some parameterizations (Belušić et al., 2007; Horvath and Vilibić, 2014; Tanaka, 2010). This indicates that conducting atmospheric simulations does not lead promptly to forecasting the occurrence of a meteo-tsunami.

## 1.4 Goal of this thesis

Although meteo-tsunami is a sometimes-devastating hazard, its forecast has not yet been made. To enhance our understanding of the amplification mechanism of meteo-tsunamis, we conduct numerical simulations to investigate the amplification mechanism

of meteo-tsunamis originating west of Kyushu Island and its universality is checked for three meteo-tsunami cases in Chapter 2. In Chapter 3, a possible forecasting system based on real-time observation of an oceanic wave and oceanic modeling is proposed. General conclusion and possible future directions are given in the final chapter.

## Figures

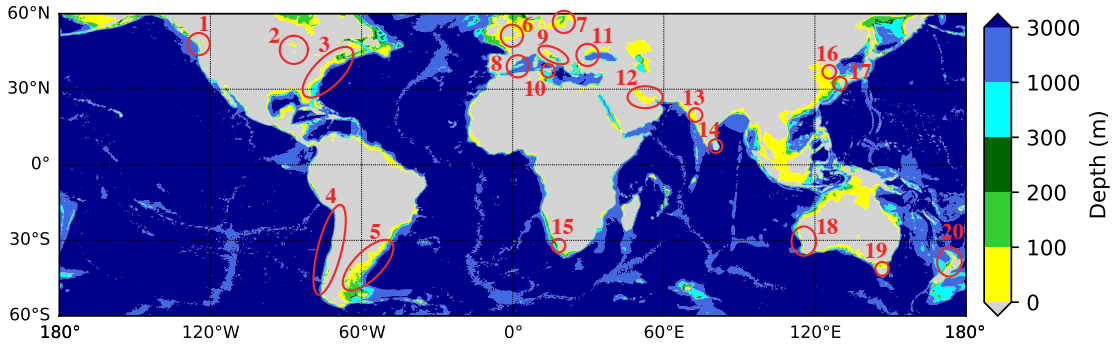


**Figure 1.1** Bathymetry (m) (color) from ETOPO1 (Amante and Eakins, 2009) and locations (surrounded by red circles) where meteo-tsunamis have been documented by the year 2019. Details of each location are shown in Table 1.1.

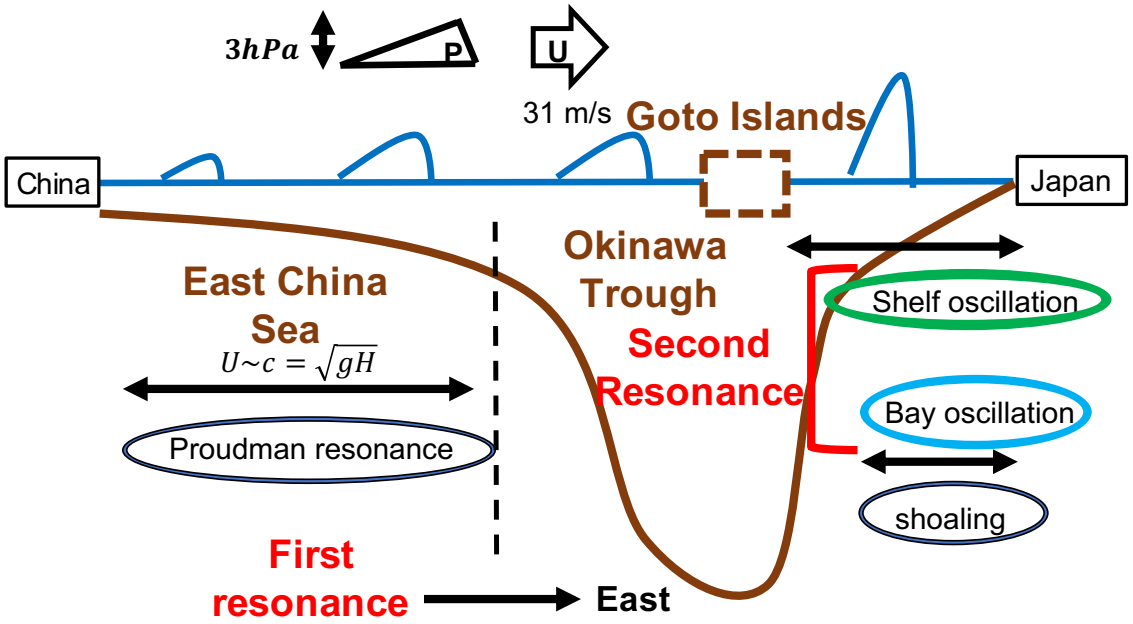


**Figure 1.2** A sketch of the amplification mechanism of the meteo-tsunami in Nagasaki Bay on March 31, 1979. The Proudman resonance (first resonance) worked over the continental shelf in the East China Sea and the resonant connection between shelf oscillations and bay oscillations were formed near the coast of Kyushu Island, Japan.

## Tables

**Table 1.1** List of areas where the occurrence of meteo-tsunamis has been reported. The numbers refer to the locations written near each circle in Figure 1.1.

| Area | Location | Local name | References |
|---|---|---|---|
| 1 | British Columbia and Washington | | Thomson et al. 2009 |
| 2 | Great Lakes | | Linares et al. 2016 |
| 3 | U.S. east coast | | Pasquet and Vilibić 2013; Wertman et al. 2014 |
| 4 | Chilean and Peruvian coasts | | Carvajal et al. 2017 |
| 5 | Buenos Aires coast | | Perez and Walter 2017 |
| 6 | Netherlands coast | | de Jong and Battjes 2004 |
| | English Channel | | Williams et al. 2019 |
| 7 | Finnish coast | seebär | Pellikka et al. 2015 |
| 8 | Coast of Balearic Islands | rissaga | Vilibić et al. 2008; Ličer et al. 2017 |
| 9 | Croatian coast | šćiga | Vilibić et al. 2006; Orlić et al. 2010; Šepić et al. 2012; Šepić et al. 2016 |
| | Italian coast | | |
| 10 | Sicily | marrobbio | Šepić et al. 2018 |
| | Malta | mulghuba | Drago 2009 |
| 11 | Bulgarian coast | | Vilibić et al. 2010 |
| 12 | Southern coast of Iran | | Heidarzadeh et al. 2019 |
| 13 | Western coast of India | | Mehra et al. 2012 |
| 14 | Western coast of Sri Lanka | | Indika et al. 2017 |
| 15 | Western coast of South Africa | | Okal et al. 2014 |
| 16 | Western coast of Korean Peninsula | | Kim et al. 2017, 2019 |
| 17 | Western coast of Kyushu, Japan | abiki | Hibiya and Kajiura 1982; Tanaka 2010 |
| 18 | Western Australian coast | | Pattiaratchi and Wijeratne 2015a |
| 19 | Tasmania | | Pattiaratchi and Wijeratne 2015b |
| 20 | Eastern seaboard of New Zealand | | Goring 2009 |

# Chapter 2

# The amplification mechanism of meteo-tsunamis originating off the western coast of Kyushu Island

Section 2.2 of this chapter has been published as:
Fukuzawa, K., and Hibiya, T. (2019), The amplification mechanism of a meteo-tsunami originating off the western coast of Kyushu Island of Japan in the winter of 2010, *J. Oceanogr.* https://doi.org/10.1007/s10872-019-00536-3

## 2.1 Introduction

In Japan, meteo-tsunamis are frequently observed on the western coast of Kyushu Island during winter–spring and are called “abiki”. The name “abiki” is related with the fact that a strong current associated with this phenomenon pulls a fishing net under the water. Maximum amplitudes of sea level oscillations associated with meteo-tsunamis have ever reached about 1 m at the tide stations in Nagasaki Bay, Makurazaki Bay, Aburatsu Bay, Ohdomari Bay, Tanegashima Island, Nakanoshima Island, Amami Island (Shiga et al., 2007) and Kami-Koshiki Island (Asano et al., 2011). In particular, Nagasaki Bay and Makurazaki Bay are representative bays that have been frequently attacked by meteo-tsunamis with the amplitudes sometimes reaching more than several meters.

Basically, frequent occurrence of large meteo-tsunamis on the western coast of Kyushu Island can be attributed to the existence of a broad continental shelf with less than 100 m depth extending more than ~500 km in the East China Sea. In such a shallow sea, the traveling speed of a shallow water wave becomes close to that of the atmospheric pressure disturbance ~100 km/h. Consequently, the oceanic waves cannot escape from the direct influence of the traveling atmospheric pressure disturbances so that they are efficiently amplified during the course of their propagation (Proudman resonance).

These shallow water waves are usually amplified up to of the order of 0.1 m before they go through the eastern edge of the continental shelf in the East China Sea and get out of the effect of atmospheric pressure disturbances. Thereafter, the shallow water waves propagate eastward as free waves and excite eigen-oscillations in various bays on the western coast of Kyushu Island. An interesting feature of the large meteo-tsunami in Nagasaki Bay that occurred on March 31, 1979 is that one of the eigen-oscillations formed on the continental shelf surrounded by the northwestern coast of Kyushu Island and the Goto Islands (Goto Nada) shared nearly the same period with the first mode oscillation in Nagasaki Bay, so that oceanic waves resonant with the eigen-oscillation in Nagasaki Bay were continuously supplied from Goto Nada (Hibiya and Kajiura, 1982). As a result, the amplitude of sea level oscillations was increased up to ~3 m at the Nagasaki tide station.

Although nearly the same local topographic amplification mechanism has been suggested for a meteo-tsunami in Makurazaki Bay, the detailed amplification mechanism

still remains to be resolved. Off Makurazaki Bay, a narrow shelf with a gentle southward slope runs west to east. Previous observational studies suggested that edge waves can explain differences in coherence and phase between sea level time series at three observation stations on this shelf (Yanuma and Tsuji, 1998; Asano et al., 2013). Although they also speculated that those edge waves might be related to the occurrence of large meteo-tsunamis in Makurazaki Bay, they did not clarify the mechanism how such edge waves contributed to the amplification of sea level oscillations.

Clarifying the universal amplification mechanism of meteo-tsunamis is requested. This chapter is organized as follows. In Section 2.2, we conduct numerical simulations to investigate the amplification mechanism of the meteo-tsunami that occurred in the winter of 2010. It was one of the largest meteo-tsunamis with the maximum amplitude of water level oscillations exceeding 1 m in both Makurazaki Bay and Nagasaki Bay. In Sections 2.3 and 2.4, the universality of the amplification mechanism explained in Section 2.2 is checked in the simulations results of two other meteo-tsunamis which occurred in the winter of 2012 and 2004. The final section provides summary of this chapter.

## 2.2 The meteo-tsunami occurred in the winter of 2010

### 2.2.1 Observation

Makurazaki Bay is a small bay with the length and width of both ~1 km. Through its mouth opened to the south, the bay is connected to the east–west elongated shelf with the zonal and meridional lengths of ~30 km and ~10 km, respectively, and the average depth of about 100 m. The shelf is blocked by Cape Kaimondake eastward.

The tide station in Makurazaki Bay is located at the innermost of the bay where the average depth is only several meters, recording sea levels at 15-second interval. Remarkable sea level oscillations were observed in the daytime on March 3, 2010. Especially large oscillations started at about 11:00 JST with the maximum range (crest to trough) exceeding 1.0 m at about 11:40 JST and about 13:30 JST on March 3. Large sea level oscillations were also observed in other bays in Kyushu Island such as Nagasaki Bay (~1.0 m) and Tanegashima Bay (~0.5 m). Remarkable water level oscillations started at about 11:30 with the maximum range of about 1.0 m at about 12:00–13:00 JST in Nagasaki Bay.

Simultaneously, a marked atmospheric disturbance with a sequence of rapid pressure changes was observed at the meteorological stations in Nagasaki, Fukue, Ushibuka, Akune, Meshima Island, and Kamikoshiki Island off the west coast of Kyushu Island (Figure 2.1 and Figure 2.2). These stations recorded the meteorological data at 1-min interval. The first sudden increase of atmospheric pressure was about 1 hPa in about 20 min as is typically seen in the data at Meshima Island. In these data, the atmospheric pressure change first occurred at Meshima Island, the westernmost station among the meteorological stations listed above, at about 9:10 JST on March 3. It was then observed at Fukue at about 9:30 JST, Kamikoshiki Island, Nagasaki, and Ushibuka at about 10:20 JST, and at Akune at about 10:30 JST, respectively, on March 3. These time lags suggest that the pressure disturbance propagated eastward. The exact lags of arrival time of the pressure disturbance from Meshima Island to the other stations are estimated by applying the lag correlation method to high-pass filtered surface pressure data by applying three times the Kolmogorov-Zurbenko (KZ) filter whose length is set to 31. The propagation speed and direction of the pressure disturbance are then calculated using the time lag from two arbitrary stations out of Fukue, Nagasaki, Ushibuka, Meshima Island, and Kamikoshiki Island to Akune and geographical distance between them to yield the propagation speed 30.7 ± 4.2 m/s and the propagation direction –15.7 ± 15.2° counterclockwise from the east (all errors here mean a standard deviation). Another method is proposed to estimate the values which give the smallest error using the least squares approach (Orlić, 1980; Šepić et al., 2009) (see Appendix A.1). The pressure disturbance was not apparent at Izuhara and Tanegashima, northernmost and southernmost meteorological stations, respectively, indicating that the lateral width of the pressure disturbance was about 350 km. The wind speed before and after the pressure change at each meteorological station did not change appreciably.

The sea level time series observed at tide stations and the surface meteorological observation data, such as surface pressure, are provided by Japan Meteorological Agency and the Satsumasendai city office.

### 2.2.2 Numerical Simulation (Ocean Model)

The ocean model used in this study is based on the linearized, depth-integrated, non-rotating, non-viscous shallow water equations of motion and continuity, because our

interest is in a barotropic ocean response. These equations are written as

$$\frac{\partial Q_x}{\partial t} = -gH\frac{\partial(\eta - \eta_a)}{\partial x} \tag{2-1}$$

$$\frac{\partial Q_y}{\partial t} = -gH\frac{\partial(\eta - \eta_a)}{\partial y} \tag{2-2}$$

$$\frac{\partial \eta}{\partial t} = -(\frac{\partial Q_x}{\partial x} + \frac{\partial Q_y}{\partial y}) \tag{2-3}$$

where $t$ is time, $x$ and $y$ denote longitude-latitude coordinates directed to the east and north, respectively. $H$ is the sea depth, $Q_x$ and $Q_y$ are $x$ and $y$ components of the depth-integrated transport, respectively, $\eta$ is the sea surface elevation anomaly, $\eta_a$ denotes the static response of the sea surface elevation to an atmospheric pressure deviation, and $g$ is the acceleration due to gravity (9.8 m/s$^2$). These equations are solved on the finite difference Arakawa-C grid by the leap-frog scheme. The Asselin time filter is used to dampen the computational mode.

This calculation includes one-way connection from larger to smaller regions. The outermost domain (Region 1) covers the East China Sea and Kyushu Island (122.0°–131.0°E and 25.0°–34.8°N) with a grid spacing of 30 arc seconds (1081×1176 grid points). The intermediate domain (Region 2) covers the near Kyushu area (129.3°–131.0°E and 30.3°–34.8°N) with a grid spacing of 10 arc seconds (615×1620 grid points), one of the innermost domains covers Nagasaki Bay (Region 3, 129.8°–129.9°E and 32.7°–32.8°N) with a grid spacing of 3.3 arc seconds (93×78 grid points) as well as Makurazaki Bay (Region 4, 130.27°–130.33°E and 31.24°–31.27°N) with a grid spacing of 2 arc seconds (110×65 grid points) (Figure 2.1). The time step of integration is taken to be 0.5 seconds in Region 1, 0.5/3 seconds in Region2, 0.5/9 seconds in Region 3 and 0.5/15 seconds in Region 4, respectively. A radiation boundary condition is imposed on the open boundary in all the domains. The domains are connected with each other through one-way nesting method, in which the information from a coarse-grid domain is given gradually to the boundary area of a fine-grid domain with a width of 10 grid points similar to Oey and Chen (1992). “JTOPO30v2” and “M7000” by Marine Information Research Center, Japan Hydrographic Association, and the data by the Central Disaster Prevention Council of Cabinet Office, Japan are used as topography data.

### 2.2.3 A model of the atmospheric pressure disturbance

To reproduce the meteo-tsunami, an accurate modeling of the propagating atmospheric pressure disturbance is indispensable. However, there is no meteorological data with high temporal resolution in the East China Sea and the atmospheric pressure data at different meteorological stations on the west coast of Kyushu Island are too complicated to be related with each other except the abrupt increases of atmospheric pressure (Figure 2.2). Bearing in mind that the main objective of the present study is to understand the amplification mechanism of the meteo-tsunami in Nagasaki Bay and Makurazaki Bay, we assume here a simple idealized model of the atmospheric pressure disturbance; it consists of a sequence of triangle-shaped rapid pressure changes in the propagation direction, taking into account the data at the westernmost meteorological station, Meshima Island (32.0˚N, 128.3˚E) (see Figure 2.3) with laterally uniform structure over its width of 350 km creating the sharp lateral edges. We assume that this atmospheric pressure disturbance propagates about 500 km over the East China Sea in a direction of -5˚ with a constant speed of ~30 m/s without change of its shape. Note that this direction -5˚ is within one standard deviation from the mean estimated in section 2.2.1 and yields the best simulation results. The sea surface elevation and water velocity are initially set to zero in the whole calculation domain. The forcing term $\eta_a$ due to atmospheric pressure is updated every 1 min in the numerical simulation. Note that the wind stress is omitted in this numerical simulation since it was not significant throughout the simulation period.

### 2.2.4 Validity of simulation results

As typical examples, the calculated and observed sea level variations at the tide stations in Nagasaki Bay and Makurazaki Bay are shown in Figure 2.4. The time adjustment of the calculated to observed data is performed based on the arrival time of the maximum atmospheric pressure anomaly at Meshima Island. The observed sea level variations are obtained by applying three times the KZ filter with a length of 65 to the observed original data. Although the calculated time series in Makurazaki Bay includes a time lag of ~5 min, it agrees fairly well with the observed one in both the amplitude and phase during the amplification phase of the meteo-tsunami. In order to quantify the accuracy of this model, the maximum amplitude of sea level variations, the lag-

correlation coefficient and root mean square error (RMSE) of the simulated amplitude and the observed amplitude are calculated (in Table 2.1) (see Appendix A.2). Wavelet power spectra (Torrence and Compo, 1998) of the calculated variations show noticeable peaks around periods of 20–40 min and 10–25 min in Nagasaki Bay and Makurazaki Bay during the amplification phase, respectively (Figure 2.5), consistent with the observation data.

### 2.2.5 The amplification process on the continental shelf in the East China Sea

Snapshots of the calculated sea level variations off the western coast of Kyushu are shown in Figure 2.6. Resonant interaction between the eastward-traveling atmospheric disturbance and the excited shallow water waves, namely, the Proudman resonance takes place in the East China Sea. The largest oceanic wave height reaches up to 0.1 m.

The calculated sea level variations along the propagation direction of the atmospheric pressure disturbance are shown in Figure 2.7. In particular, the oceanic waves excited by the rear part of the atmospheric pressure disturbance with the steepest pressure gradient are amplified with time due to the Proudman resonance. Although the front of the oceanic waves is in phase with that of the atmospheric pressure disturbance in the first and second panels, the last panel indicates that the oceanic wave is getting out of the influence of the atmospheric pressure forcing (Figure 2.7).

The numerical simulation shows that oceanic waves with periods of 20–40 min played an essential role in exciting the meteo-tsunami in Nagasaki Bay in 2010 (Figure 2.5). A wavelet power spectrum of the sea level variations at the entrance of Nagasaki Bay in Region 1 shows noticeable peak around periods of 20–40 min during the amplification phase in Nagasaki Bay (Figure 2.8(a)). This indicates that the amplification mechanism explained by Hibiya and Kajiura (1982) worked also in the 2010 meteo-tsunami; one of the eigen-oscillations formed on the continental shelf in Goto Nada shares nearly the same period with the first mode oscillation in Nagasaki Bay, so that oceanic waves resonant with the first mode oscillation in Nagasaki Bay are continuously supplied. In the following sections, the amplification mechanism of the meteo-tsunami in Makurazaki Bay is discussed.

### 2.2.6 Oceanic waves on the continental shelf off Makurazaki Bay (edge waves)

The numerical simulation shows that oceanic waves with periods of 10–25 min played an essential role in exciting the meteo-tsunami in Makurazaki Bay in 2010. After oceanic waves arrive at the western coast of Kyushu Island near Makurazaki Bay, part of the waves continues to propagate eastward on the shelf running east-west off Makurazaki Bay. A snapshot of sea surface height and velocity vectors at the time when the largest oceanic wave arrives at the coast is shown in Figure 2.9(a). The distribution of sea surface height exhibits the features of edge waves, namely, the decaying behavior offshore and wave-like behavior along the coast with the velocity field refracted toward the coast.

For the linearized, non-rotating, non-viscous shallow water equations of motion and continuity, an analytical solution of an edge wave propagating along the coastline in the $x$ direction on a shelf with a constant slope, $\alpha$, in the $y$ direction can be expressed as

$$\eta = F \cdot e^{-ky} e^{i(kx-\omega_n t)} \tag{2-4}$$

$$u = \frac{gk}{\omega_n} \cdot F \cdot e^{-ky} e^{i(kx-\omega_n t)} \tag{2-5}$$

$$v = i\frac{gk}{\omega_n} \cdot F \cdot e^{-ky} e^{i(kx-\omega_n t)} \tag{2-6}$$

$$\omega_n{}^2 = gk(2n+1)\alpha \tag{2-7}$$

where $F$ is the amplitude of sea level anomaly, $k$ is the wavenumber, $\omega_n$ is the corresponding frequency with n the number of nodal lines parallel to the coast (LeBlond and Mysak, 1981). The analytical solution of the lowest mode ($n=0$) with a wavelength of 60 km and a period of 23 min on a shelf with the southward slope of 0.02 is shown in Figure 2.9(b). Although not only edge waves but also free waves are included in the snapshot of Figure 2.9(a), we can see that edge waves are propagating eastward on the narrow shelf off Makurazaki Bay with a dominant period of about 25 min, consistent with the analytical value.

### 2.2.7 Additional experiments focusing on the oscillations on the shelf off Makurazaki Bay

Following Loomis (1966) (see Appendix A.3), we numerically solve the eigenvalue problem for the narrow continental shelf off Makurazaki Bay, using topographic data with a resolution of 600 m (120×90 grid points) from “M7000”. Three

eigen-modes are shown in Figure 2.10. The spatial patterns of sea level of these modes have the characteristics of an edge wave mentioned above, indicating that these eigen-oscillations are created by edge waves. In addition, the spatial patterns of all modes have a nodal line near Cape Noma, where the on-offshore slope of the shelf significantly changes (Figure 2.11(a)).

In order to examine the amplification mechanism of the oceanic waves on the narrow continental shelf off Makurazaki Bay, we conduct additional numerical experiments in which the model domain is limited to a small area including Makurazaki Bay (Figure 2.11(a)) so that it can be covered with a grid spacing of 200 m (430 × 300 grid points). Periodic sinusoidal disturbances with an amplitude of 1.0 m and a period of 10 to 25 min at 1-min intervals are continuously given at each station western off the shelf denoted by a circle in Figure 2.11(a).

After the eastward propagating oceanic waves arrive at Cape Kaimondake (Figure 2.11(a)), part of the waves is reflected back westward and interferes constructively with the incident oceanic waves to create a standing oscillation on the shelf. The resulting spatial patterns of the maximum wave heights are displayed in Figure 2.12(a). The distance between adjoining anti-nodes (or nodes) representing a half-wavelength of the periodic oscillations is estimated to be about 20, 30 and 34 km for periods of 12, 16 and 18 min, respectively.

In all the cases, the amplitudes of the waves are largest at the coast and gradually decrease southward, which is attributed to the features of edge waves. The southward slope of the shelf off Makurazaki Bay is steep near the coast and gentle in the middle of the shelf, with the average slope of 0.014–0.025. Substituting the simulated wavelengths of 20, 30 and 34 km for the oceanic waves with the corresponding periods of 12, 16 and 18 min into the dispersion relation (2-7), gives the bottom slope $\alpha$ = 0.025, 0.020, and 0.019, respectively, which fall within the range of the actual southward slope of the shelf. Furthermore, the estimated southward slope tends to be steeper as the forcing period becomes shorter, which is again explained in terms of the edge waves because they are more strongly trapped on the steeper coastal slope with smaller cross-shore structures as their periods become shorter. These results are consistent with the characteristics of edge waves.

When the forcing period is 12 min (16–18 min), the third (second) anti-node, numbered from the eastward end, is found near the bay. In such cases, the amplified oceanic waves are expected to enter Makurazaki Bay efficiently resulting in large sea level oscillations in Makurazaki Bay.

In order to confirm the importance of the existence of Cape Kaimondake, we further carry out numerical experiments removing Cape Kaimondake and extending the shelf eastward to the open boundary (Figure 2.11(b)). In this case, oceanic waves propagate radially from the western edge of the shelf and eastward-propagating waves continue to travel eastward, so that anti-nodes and nodes are not created at all (Figure 2.12(b)). The ratio of the maximum amplitude of sea level oscillations with Cape Kaimondake to that without Cape Kaimondake is a function of wave period. Near Makurazaki Bay, the ratios become large at periods of 12 and 16 min with the corresponding amplification factors of 1.5 and 2, respectively (Figure 2.13 (b)). The areas with the ratios exceeding unity, in the case of periods of 12, 16 and 18 min, are located on the shelf off Makurazaki Bay and other areas around Cape Noma, coinciding with the areas of the anti-nodes of eigen-oscillations, which indicates that these significant oscillations are created by the existence of Cape Kaimondake. Oceanic waves with periods longer than 20 min, on the other hand, propagate away without being effectively reflected, because they have too large cross-shore structures to be blocked by Cape Kaimondake, so that the ratio is nearly unity.

Now, we evaluate the growth of the oceanic waves on the shelf off Makurazaki Bay, regarding this area as a semi-closed system that traps the waves at a certain ratio $r$ ($0 < r < 1$) during each period. The amplification factor of a sea level oscillation $A$ can then be written as

$$A = \frac{1 - r^t}{1 - r} \tag{2-8}$$

$$= \frac{1}{1 - r}\{1 - exp(ln\, r \cdot t)\} \tag{2-9}$$

$$= \frac{1}{1 - r}\{1 - exp(-\zeta \cdot \tau \cdot t)\} \tag{2-10}$$

where $t$ is the time normalized by the forcing period $\tau$ and $\zeta$ is a damping coefficient. This formulation, consistent with that suggested by Bellotti (2007), is applied to a time series

of sea level oscillations at the location near the entrance of Makurazaki Bay (drawn as a gray circle in Figure 2.13(a)) during its amplification phase. Figure 2.14(a) shows the damping coefficient against the forcing period. The consistent relationship between $\zeta$ and maximum amplitudes indicates the validity of this formulation. For a forcing period longer than 20 min, the damping coefficient monotonically increases (not shown). There are two ranges of periods, 10–12 and 15–19 min, for which the damping coefficient is small. As a typical example, the average damping coefficient $\zeta$ (the trapping ratio per one cycle, $r$) near Makurazaki Bay is about 0.029 rad/min (0.71) at a period of 12 min and about 0.031 rad/min (0.61) at a period of 16 min, indicating that 90% of the saturated amplitude is attained after ~7 and ~5 cycles ($-\ln(0.10)/\zeta$) at the respective period.

### 2.2.8 Additional experiments focusing on the resonance mechanism in Makurazaki Bay

Again following Loomis (1966), we numerically solve the eigenvalue problem for Makurazaki Bay, using topographic data with a resolution of 30 m (80×90 grid points) from the data set constructed by the Central Disaster Prevention Council of Cabinet Office, Japan. The lowest two modes are shown in Figure 2.15. These modes can resonantly interact with the lateral oscillations on the offshore shelf with the periods of 12 and 16 min, respectively.

In order to evaluate the resonance between the oscillations in Makurazaki Bay and on the offshore shelf, we carry out additional numerical experiments by restricting model domain to a small area including Makurazaki Bay so that it can be covered with a fine grid spacing of 30 m (110 × 90 grid points in the longitudinal and latitudinal directions, respectively). Periodic plane sinusoidal disturbances with an amplitude of 0.010 m and a period of 10 to 20 min at 1-min intervals are continuously given at the south boundary of the domain.

The damping coefficient $\zeta$ of the sea level oscillation at the Makurazaki tide station is estimated as shown in Figure 2.14(b). The maximum amplitude of sea level oscillations and the minimum value of $\zeta$ both occur at periods of 16 and 12 min. This means that, when oceanic waves with periods of about 16 and 12 min are imposed on the narrow shelf off Makurazaki Bay, large sea level oscillations must be excited in the bay. The minimum value of $\zeta$ and the maximum trapping ratio per one cycle, $r$, are 0.015

rad/min (0.014 rad/min) and 0.79 (0.84), respectively, when oceanic waves with a period of 16 min (12 min) are continuously available; the 90% of the saturated amplitude is attained after ~10 cycles (~14 cycles). Although the 2010 meteo-tsunami was excited mainly by oceanic waves with a period of about 16 min, there exist some meteo-tsunamis ever excited by oceanic waves with a period of about 12 min as reported by Shiga et al. (2007).

Although the combined amplification factor of the oscillation in Makurazaki Bay and on the offshore shelf (see Figure 2.14(a), (b)) is nearly the same at periods of 12 and 16 min, the combined damping factor of the oscillation at a period of 12 min is smaller than that at a period of 16 min. This means that the saturation of bay oscillation can be attained by the smaller number of incident oceanic waves at a period of 16 min. This suggests that large meteo-tsunamis in Makurazaki Bay are more frequently excited at a period of 16 min than at a period of 12 min. This speculation, however, should be checked for many meteo-tsunami cases in the future.

### 2.2.9 Additional experiments focusing on the oscillations on the shelf off Nagasaki Bay

In order to examine the amplification mechanism of the oceanic waves on the shelf region off Nagasaki Bay, Goto Nada, we perform additional numerical experiments in which the model domain is limited to the small area (128.5°–130.3°E and 32.1°–33.7°N) so as to be covered with a grid spacing of 30 arc seconds (221 and 201 grid points in the longitudinal and latitudinal directions, respectively) (Figure 2.16(a)). Periodic sinusoidal disturbances with an amplitude of 1.0 m and a period of 20 to 70 minutes at 5-minute intervals are continuously given at the just offshore of Nagasaki Bay.

After the excited oceanic waves propagate westward over the shelf and arrive at coastal areas, part of the waves is reflected back eastward while the other part is radiated. The incident and reflected oceanic waves are all piled up causing a standing oscillation on the shelf region. The spatial patterns of wave heights in an oscillatory steady-state are displayed in Figure 2.17. Standing oscillations with periods of 25–35 min and 60–65 min have an antinode at the offshore of Nagasaki Bay.

In order to confirm the importance of the existence of the islands located east and north of Nagasaki Bay, we further conduct numerical experiments artificially

removing these islands and smoothly extending the shelf to the westward and northward open boundary (Figure 2.16(b)). Forced waves propagate radially from the vicinity of the entrance of Nagasaki Bay and westward-propagating (northward-) waves continue to travel westward (northward), so that anti-nodes and nodes do not appear in the experiments without the islands (Figure 2.18). The ratio of the maximum amplitude of sea level oscillations with the islands to that without the islands is a function of period (Figure 2.19). In the ratio near the entrance of Nagasaki Bay, remarkable peaks are found at 35 minutes and 60 minutes with the corresponded amplification factors of about 2.1 and 2.2. If ocean waves with these periods travel into Nagasaki Bay area, these waves are reflected, propagate westward (northward) and reflected eastward (southward) at Goto Islands (the narrow topography near Hirado Island) causing large sea level oscillations in Nagasaki Bay.

The damping coefficient $\zeta$ of the sea level oscillation at the entrance of Nagasaki Bay is estimated as shown in Figure 2.20(a). The maximum amplitude of sea level oscillations and the minimum value of $\zeta$ both occur at periods of 30 and 60 min. This means that, when oceanic waves with periods of about 30 and 60 min are imposed on the continental shelf in Goto Nada, large sea level oscillations must be excited. The minimum value of $\zeta$ and the maximum trapping ratio per one cycle, $r$, are 0.0080 rad/min (0.0044 rad/min) and 0.79 (0.77), respectively, when oceanic waves with a period of 30 min (60 min) are continuously available; the 90% of the saturated amplitude is attained after ~10 cycles (~9 cycles).

### 2.2.10 Additional experiments focusing on the resonance mechanism in Nagasaki Bay

In order to evaluate the resonant coupling between the oscillations in Nagasaki Bay and on the offshore shelf, we carry out additional numerical experiments by restricting model domain to a small area including Nagasaki Bay, Region 3 mentioned in Section 2.2.2. Periodic plane sinusoidal disturbances with an amplitude of 0.010 m and a period of 10 to 40 min at 1-min intervals are continuously given from the west boundary of the domain.

The damping coefficient $\zeta$ of the sea level oscillation at the Nagasaki tide station is estimated as shown in Figure 2.20(b). The maximum amplitude of sea level oscillations

and the minimum value of ζ both occur at periods of 30 and 18 min. This means that, when oceanic waves with periods of about 30 and 18 min are imposed on the narrow shelf off Nagasaki Bay, large sea level oscillations must be excited in the bay. The minimum value of ζ and the maximum trapping ratio per one cycle, *r*, are 0.027 rad/min (0.028 rad/min) and 0.44 (0.60), respectively, when oceanic waves with a period of 30 min (18 min) are continuously available; the 90% of the saturated amplitude is attained after ~3 cycles (~5 cycles).

### 2.2.11 The amplification mechanism of the 2010 meteo-tsunami

Wavelet spectra of sea level variations at the Nagasaki tide station and at its entrance in Region 1 share noticeable peaks around periods of 20–40 min during the amplification phase (Figure 2.8(a)). This indicates that the amplification mechanism, resonant coupling, worked in the 2010 meteo-tsunami; one of the eigen-oscillations formed on the continental shelf in Goto Nada shares nearly the same period with the first mode oscillation in Nagasaki Bay, so that oceanic waves resonant with the lowest mode oscillation in Nagasaki Bay are continuously supplied.

In Makurazaki Bay, large oscillations start at about 11:00 JST with the maximum range (crest to trough) exceeding 0.1 m at about 11:20 JST at the bay mouth (Figure 2.21(a)). Band-pass filtered sea level variations on a transect along the coastline around Makurazaki Bay are shown against time in Figure 2.21 (b). We can see that the first oceanic wave amplified through the coupling to the atmospheric pressure disturbance is incident on the shelf at 11:20 JST; it then excites sea level oscillations in Makurazaki Bay which are maintained until about 12:30 JST because of the small value of ζ (Figure 2.4(b)). After 12:30 JST, eigen-oscillations of periods 16–18 min with an anti-node around 130.3˚E are created on the offshore shelf, supplying oceanic waves that are resonant with eigen-oscillations in Makurazaki Bay consistent with Figure 2.8(b). Again, reflecting the small value of ζ, the amplitude of sea level oscillations in Makurazaki Bay rapidly grows during which period about four resonant oceanic waves were supplied.

We can further confirm the importance of Cape Kaimondake via the comparison of calculated results of the 2010 meteo-tsunami with and without Cape Kaimondake. The bathymetry without Cape Kaimondake assumes the shelf running east-west off Makurazaki Bay smoothly connected to the eastern channel, the entrance of Kagoshima

Bay. The amplitude of calculated sea level oscillations at the Makurazaki tide station without Cape Kaimondake remains similar to that with Cape Kaimondake until the first largest wave appears at about 11:40 JST but becomes less than half of that with Cape Kaimondake after 12:00 JST (Figure 2.22(a)). Furthermore, the significant spectral peak at periods of 10–25 min during the second amplification phase (about 13:00–14:00 JST) (Figure 2.5) disappears when Cape Kaimondake is removed (Figure 2.22(b)). These results indicate that Cape Kaimondake located at the eastern end of the shelf plays a key role in reflecting and providing resonant oceanic waves to Makurazaki Bay.

It should be noted that the atmospheric pressure disturbance is highly idealized in this study; with a laterally uniform structure, the atmospheric disturbance is assumed to propagate a long distance, say, about 500 km without change of its shape, which might be responsible for slight phase difference (~5 min) between the calculated and observed sea level oscillations in Makurazaki Bay. In order to check the validity of these assumptions, the numerical simulation of generation and propagation of the atmospheric pressure disturbance is desirable in the future (e.g. Tanaka, 2010; Belušić et al., 2007) because there exist limited atmospheric observation data in the East China Sea.

## 2.3 The amplification mechanism of the meteo-tsunami in 2012

本節については、５年以内に雑誌等で刊行予定のため、非公開。

## 2.4 The amplification mechanism of the meteo-tsunami in 2004

本節については、５年以内に雑誌等で刊行予定のため、非公開。

## 2.5 Conclusion

In this chapter, we have carried out numerical simulations to investigate the amplification mechanism of typical meteo-tsunamis in the winter of 2010, 2012 and 2004 that caused large sea level oscillations along the west coast of Kyushu Island such as Nagasaki Bay and Makurazaki Bay. It has been shown that the shelf region surrounded by the northwestern coast of Kyushu Island and the Goto Islands (Goto Nada) plays an

important role by creating oceanic waves with periods of 20–40 min that are resonant with eigen-oscillation in Nagasaki Bay.

In Makurazaki Bay, on the other hand, significant spectral peaks have been found at periods of 10–25 min during the amplification phase of water level oscillations, indicating that oceanic waves with these periods are strongly related to the meteo-tsunami. Additional numerical experiments have shown that edge waves repeat eastward-westward reflections on the elongated shelf between Cape Kaimondake and Cape Noma, gradually creating lateral eigen-oscillations, which can supply resonant oceanic waves with periods of 12 and 16 min to Makurazaki Bay (schematically shown in Figure 2.35).

Finally, to summarize the amplification scenario of the three meteo-tsunamis discussed so far, we calculate power spectra of sea level variations at locations marked by red circles in Figure 2.1 as well at the tide stations in Nagasaki Bay and Makurazaki Bay (Figure 2.36). We can find significant spectral peaks at a frequency of ~0.03 cycles/min at the Nagasaki tide station and at frequencies of 0.05–0.07 and 0.075–0.09 cycles/min at the Makurazaki tide station. During the course of propagation from the East China Sea to the tide stations, oceanic waves with these frequencies become resonant with eigen-oscillations on the shelf as well as in the bay so that efficient amplification takes place.

Needless to say, we must check the universality of the amplification mechanism of meteo-tsunamis clarified in this study by carrying out more case studies. Furthermore, considering that the results of this study are subject to the uncertainty of its temporal and spatial structure as mentioned already, the numerical simulation of generation and propagation of the atmospheric pressure disturbance is desirable in the future. Such numerical simulations are also useful to clarify the relationship between large-scale atmospheric pattern and small-scale atmospheric pressure disturbances, which will help us to construct the prediction system for meteo-tsunamis originating off the western coast of Kyushu Island.

## Figures

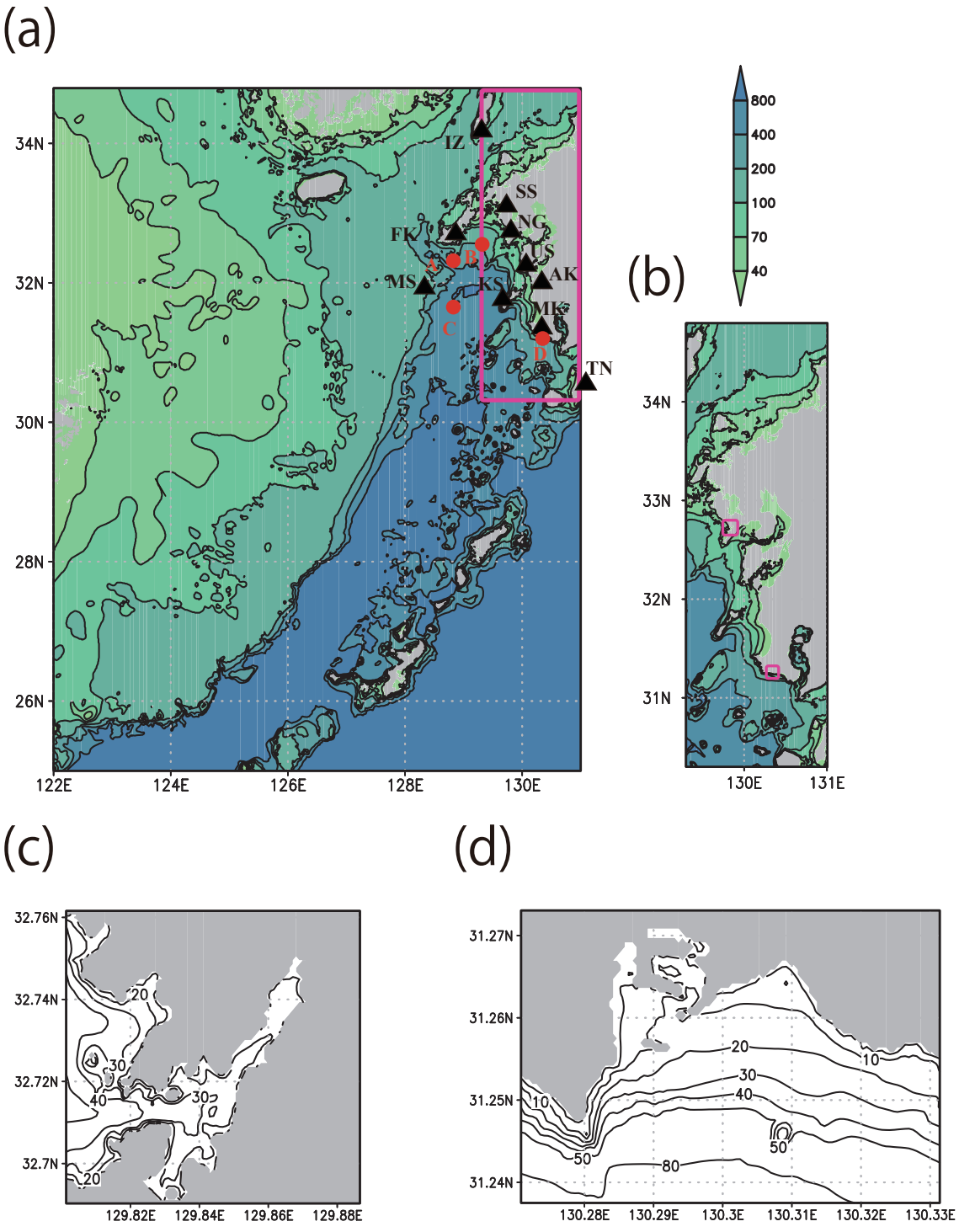
(a)
34N
32N
30N
28N
26N
122E
124E
126E
128E
130E
IZ
SS
NG
FK
TS
AK
MS
KS
MK
TN
A
B
C
D
800
400
200
100
70
40
(b)
34N
33N
32N
31N
130E
131E
(c)
32.76N
32.74N
32.72N
32.7N
129.82E
129.84E
129.86E
129.88E
20
30
40
30
20
(d)
31.27N
31.26N
31.25N
31.24N
130.28E
130.29E
130.3E
130.31E
130.32E
130.33E
10
20
30
40
50
10
50
80

**Figure 2.1** Bathymetry (m) of the outermost calculation domain around the East China Sea (a), the intermediate domain covering the near Kyushu area (b), one of the innermost domains covering Nagasaki Bay (c) and the other one covering Makurazaki Bay (d). Magenta rectangles denote inner domains. Triangles denote meteorological stations (IZ, Izuhara; SS, Sasebo; NG, Nagasaki; FK, Fukue; US, Ushibuka; AK, Akune; MS, Meshima Island; KS, Kamikoshiki Island; MK, Makurazaki; TN, Tanegashima) and there are tidal stations nearby as for NG, FK and MK. The reference Locations A (128.7˚E, 32.5˚N), B (129.0˚E, 32.6˚N), C (128.7˚E, 31.8˚N) and D (130.3˚E, 31.2˚N) for Figure 2.36 are denoted by red circles in panel (a). From Fukuzawa and Hibiya (2019).

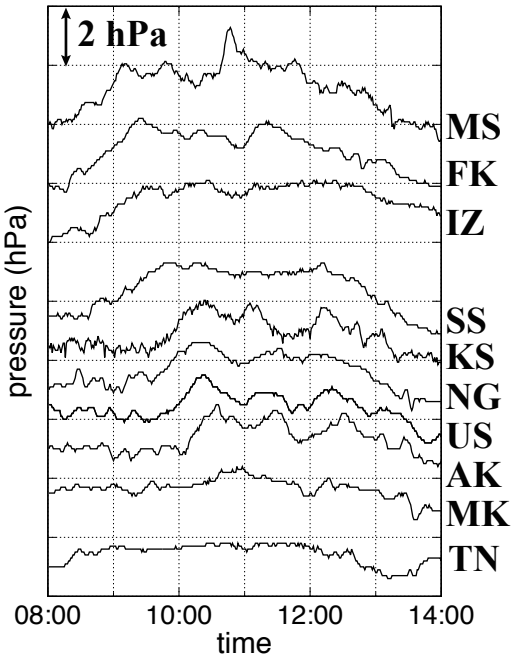


**Figure 2.2** Time series of the atmospheric surface pressure measured from 8:00 to 14:00 on March 3, 2010 at stations (MS; FK; IZ; SS; KS; NG; US; AK; MK; TN) with 1-min interval. The scale of the vertical axis is 2 hPa. From Fukuzawa and Hibiya (2019).

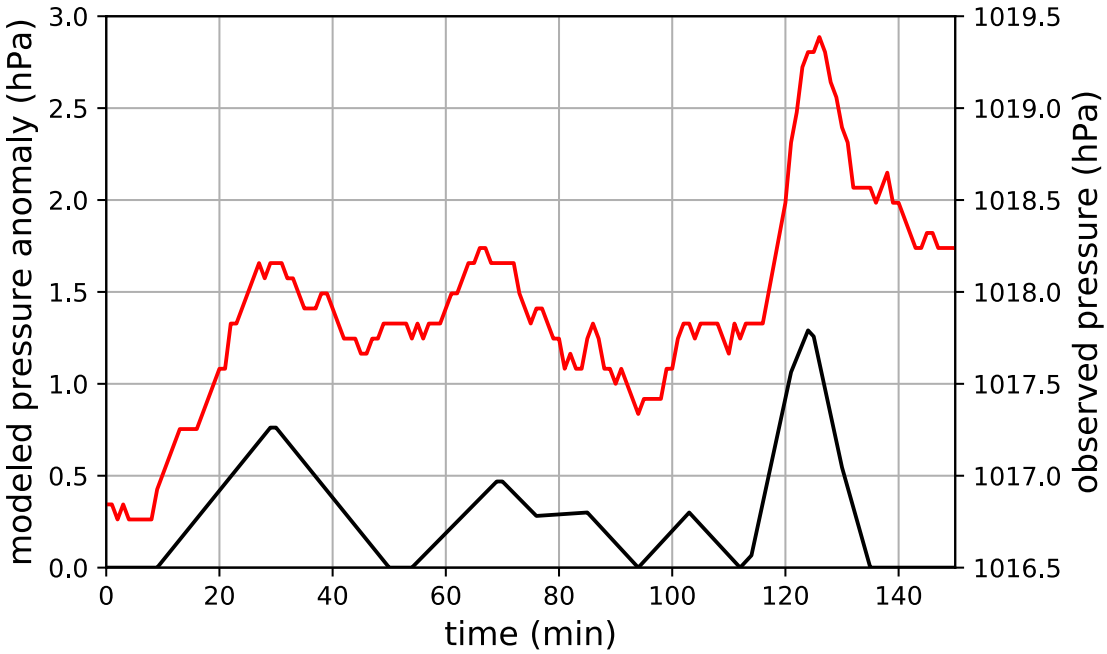


**Figure 2.3** Time series of surface pressure anomaly given to the ocean model as a driving force in the 2010 case study (black line) and time series of surface pressure observed at Meshima Island (red line). From Fukuzawa and Hibiya (2019).

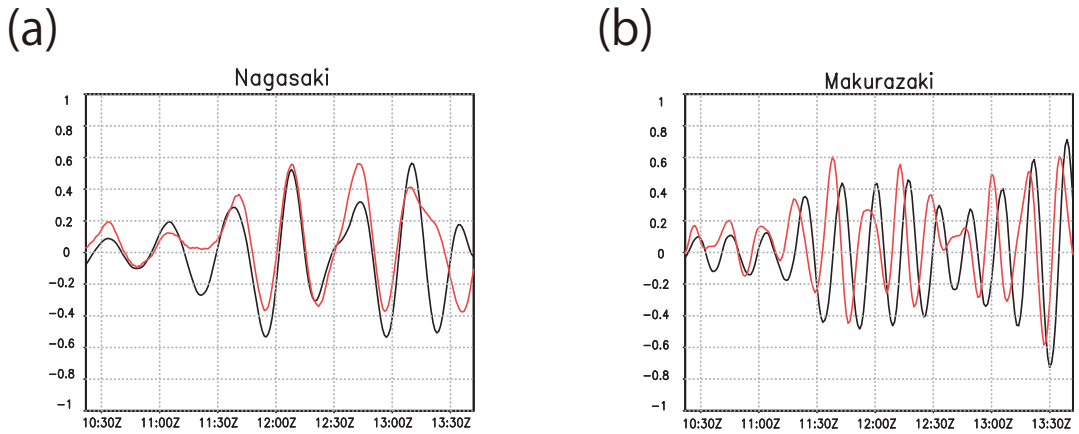


**Figure 2.4** Simulated sea level variations (m) (black line) at the tide station in Nagasaki Bay (a) and Makurazaki Bay (b). The observed ones are denoted by red lines. From Fukuzawa and Hibiya (2019).

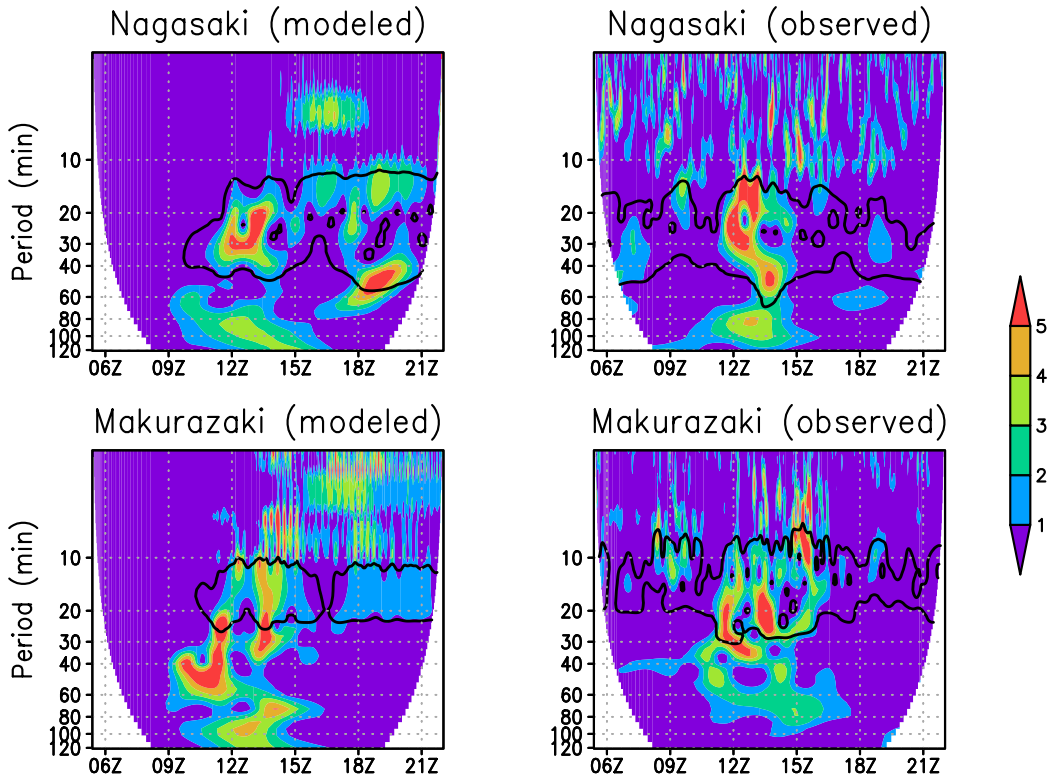


**Figure 2.5** Wavelet spectra (using the Morlet wavelet) of sea level during numerical calculation at tidal stations in Nagasaki Bay (upper left panel) and in Makurazaki Bay (lower left panel). Spectra of observed sea level in Nagasaki Bay (upper right panel) and in Makurazaki Bay (lower right panel). Color shading represents the wavelet power. Solid black line contours enclose regions of greater than 95 % confidence level for a red noise process.

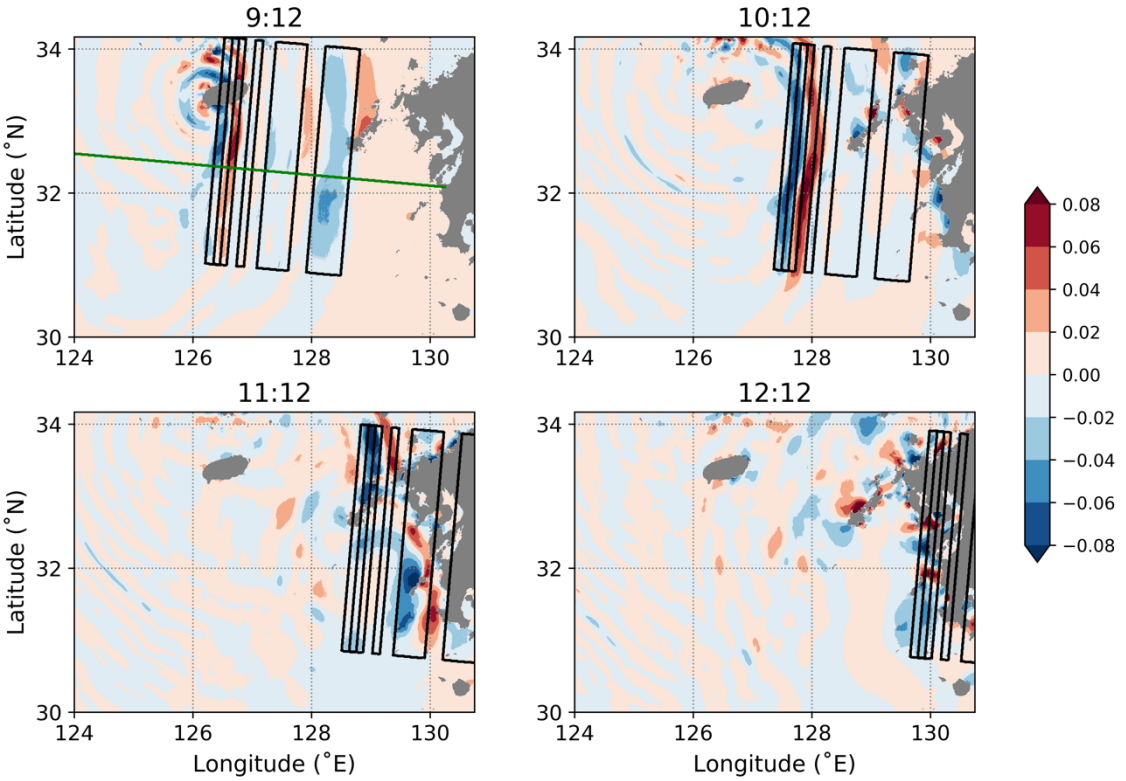


**Figure 2.6** Simulated sea level variations (m) (colors) at 9:12 JST(a), 10:12 JST(b), 11:12 JST(c) and 12:12 JST(d). Black contour lines denote the atmospheric pressure disturbance (0.2 and 1.0 hPa). The cross-section for Figure 2.7 is denoted by a green line in panel (a). From Fukuzawa and Hibiya (2019).

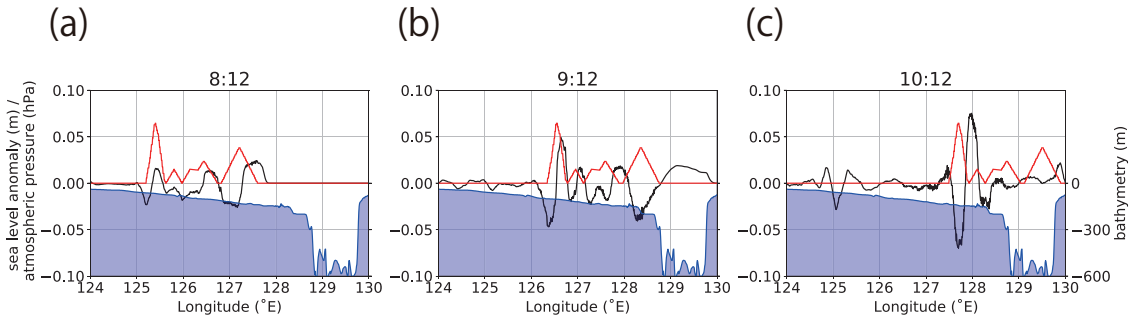


**Figure 2.7** Typical profile of the calculated sea level variations (m) (black lines) in the direction of atmospheric pressure forcing multiplied by $5 \times 10^{-2}$ (hPa) (red lines) on a transect (drawn as a green line in Figure 2.6(a)), and the bathymetric profile (m) (blue lines and shades) at 8:12 JST(a), 9:12 JST(b) and 10:12 JST(c). From Fukuzawa and Hibiya (2019).

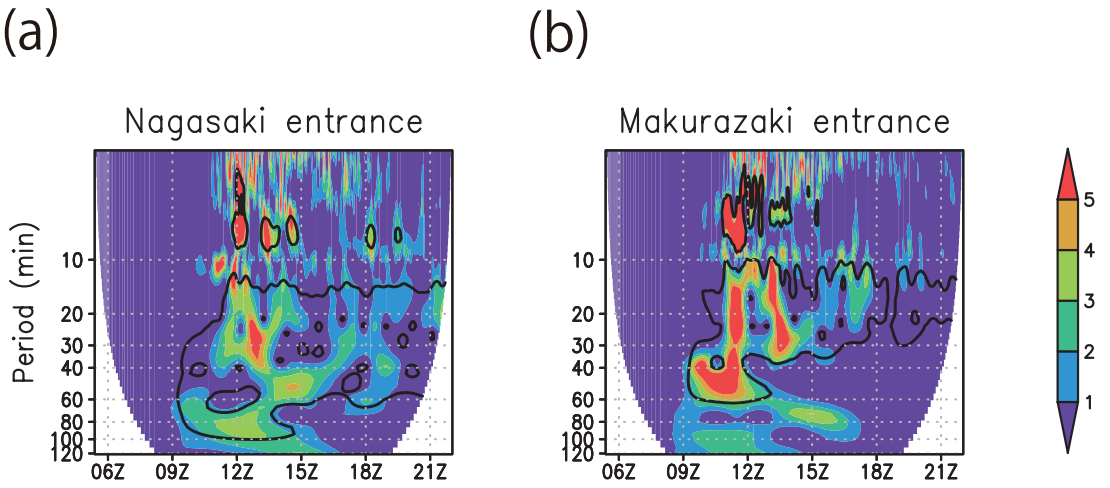


**Figure 2.8** Wavelet spectra (using the Morlet wavelet) of sea level during numerical calculation at the entrance of Nagasaki Bay (a) and Makurazaki Bay (b). Color shading represents the wavelet power. Solid black line contours enclose regions of greater than 95 % confidence level for a red noise process.

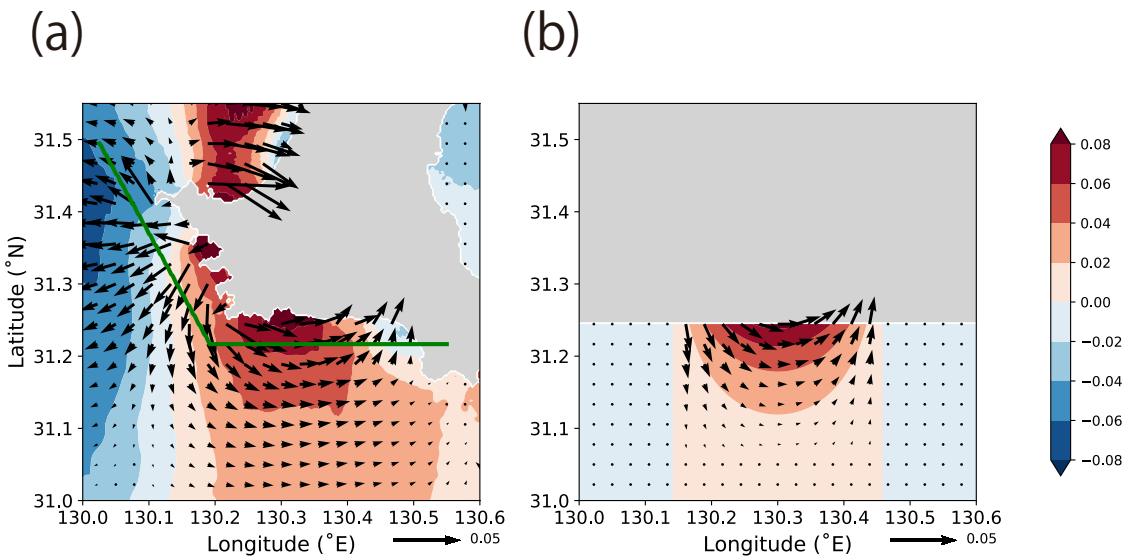


**Figure 2.9** Simulated sea level variations (m) (colors) and velocity (m/s) (vectors) at the time when the leading oceanic wave reaches the continental shelf running east-west off Makurazaki Bay (a). Analytical sea level variations (m) (colors) and velocity (m/s) (vectors) of an edge wave with a wavelength 60 km on an ideal shelf running east-west with southward slope of 0.02 (b). The cross-section for Figure 2.21 denoted by a green line in panel (a). From Fukuzawa and Hibiya (2019).

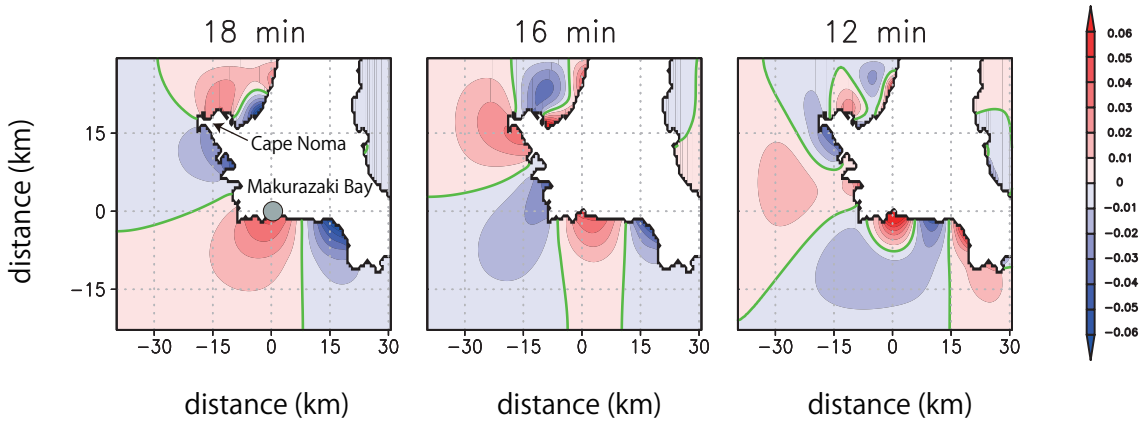


**Figure 2.10** Patterns of eigen-oscillations of sea level on the continental shelf off Makurazaki Bay with periods of 18, 16 and 12 min. Numerals on the horizontal (vertical) axis denote the eastward (northward) distance (km) from Makurazaki Bay. Color shading denotes sea level. Gray circle indicates the location of Makurazaki Bay. Green contour lines denote node lines. From Fukuzawa and Hibiya (2019).

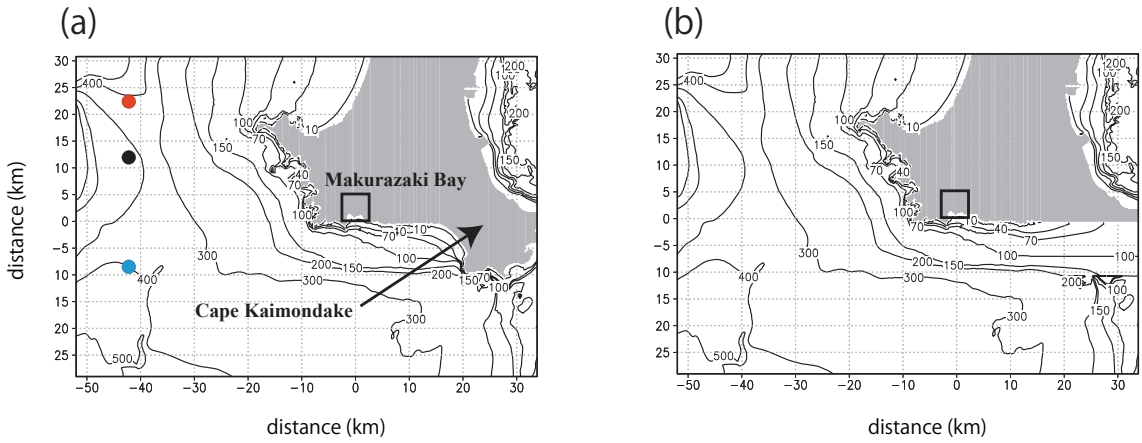


**Figure 2.11** Bathymetry (m) near Makurazaki Bay with Cape Kaimondake, original one, (a) and without Cape Kaimondake (b). Numerals on the horizontal (vertical) axis denote the eastward (northward) distance (km) from Makurazaki Bay. The locations where the periodic forcing is given are denoted by color circles (black one, Location 1; red one, Location 2; blue one, Location 3) in the left panel. From Fukuzawa and Hibiya (2019).

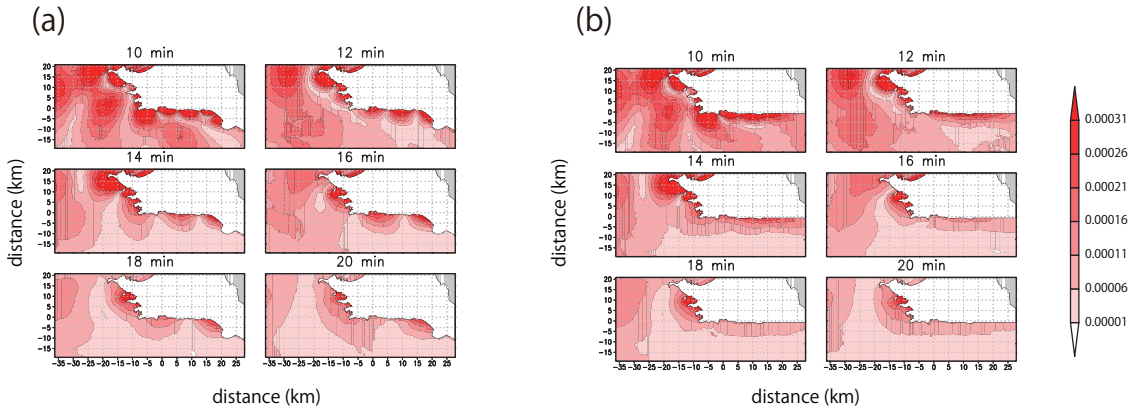


**Figure 2.12** Distributions of maximum wave heights (m) formed by periodic driving forces at Location 1 with periods of 10, 12, 14, 16, 18 and 20 min with Cape Kaimondake (a). Distributions of maximum wave heights (m) formed by periodic driving forces with periods of 10, 12, 14, 16, 18 and 20 min without Cape Kaimondake (b). From Fukuzawa and Hibiya (2019).

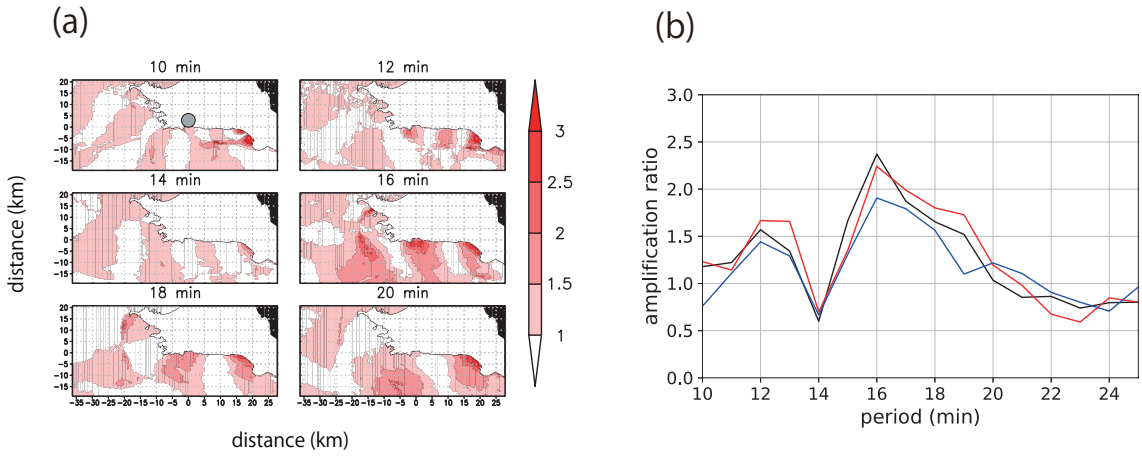


**Figure 2.13** Distributions of the ratio of maximum waves heights with Cape Kaimondake (Figure 2.12(a)) to those without Cape Kaimondake (Figure 2.12(b)) (a). The ratio of maximum amplitude of sea level oscillations near Makurazaki Bay (gray circle in the left panel) formed by periodic driving forces (black one, at Location 1; red one, at Location 2; blue one, at Location 3) with periods of 10–25 min with Cape Kaimondake to that without Cape Kaimondake (b). From Fukuzawa and Hibiya (2019).

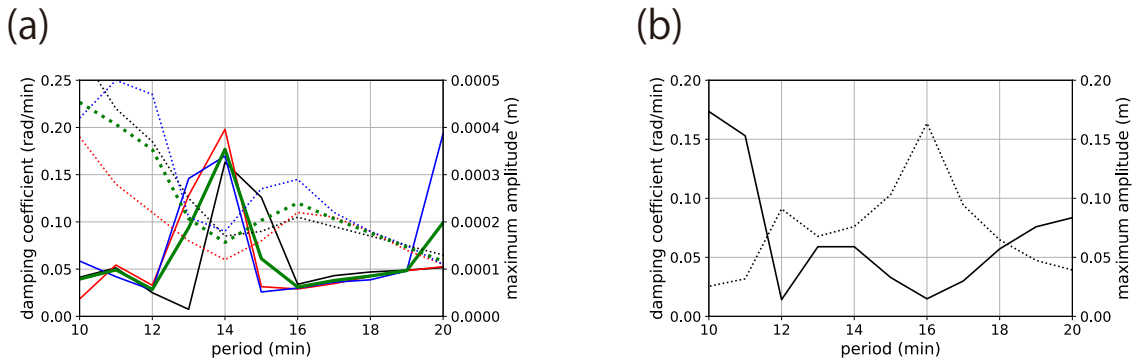


**Figure 2.14** Computed damping coefficient (solid line) and maximum sea level oscillation's amplitude (broken line), as a function of period (min) near Makurazaki Bay (black line, forced at Location 1; red line, forced at Location 2; blue line, forced at Location 3; green line, mean of three cases) (a). Computed damping coefficient (solid line) and maximum sea level oscillation's amplitude (broken line), as a function of period (min) at the Makurazaki tide station (b). From Fukuzawa and Hibiya (2019).

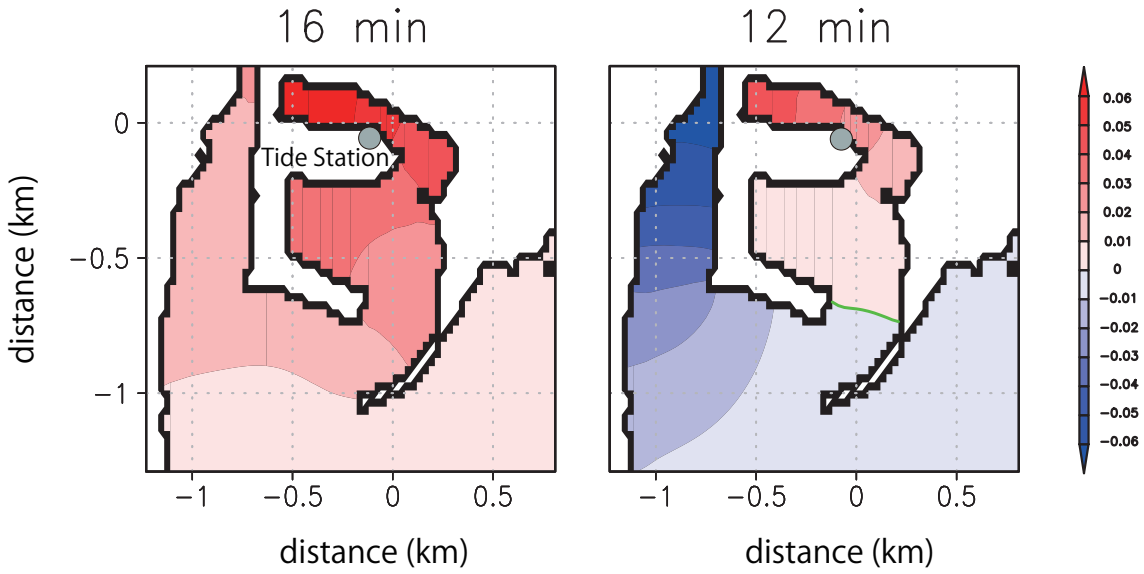


**Figure 2.15** Patterns of eigen-oscillations of sea level in Makurazaki Bay with periods of 16 and 12 min. Numerals on the horizontal (vertical) axis denote the eastward (northward) distance (km) from the Makurazaki tide station. Color shading denotes sea level. Gray circles indicate the location of the Makurazaki tide station. Green contour lines denote node lines. From Fukuzawa and Hibiya (2019).

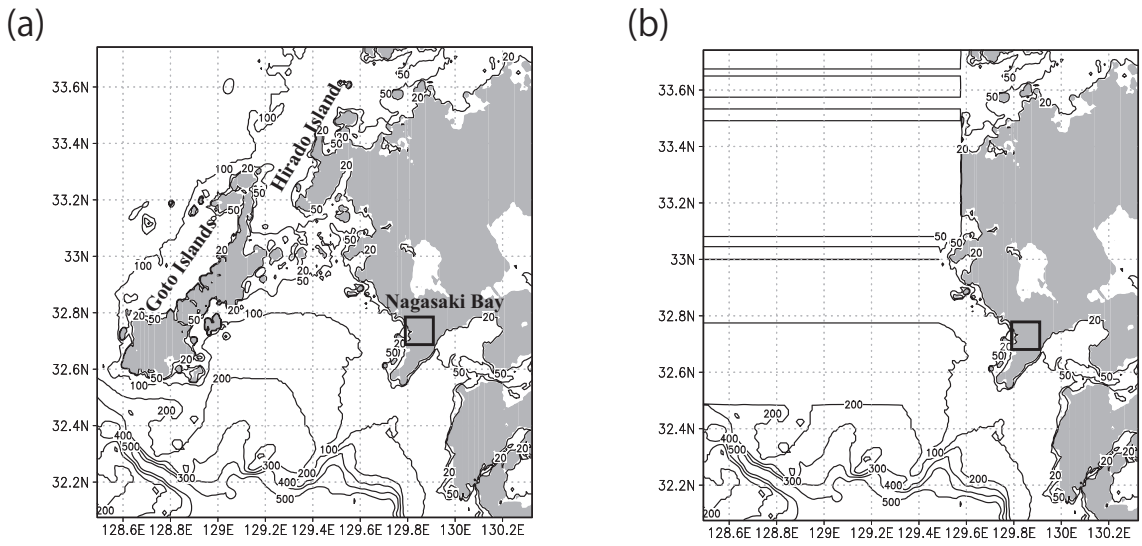


**Figure 2.16** Bathymetry (m) near Nagasaki Bay with the islands located west and north of Nagasaki Bay, original one, (a) and without the islands located west and north of Nagasaki Bay (b).

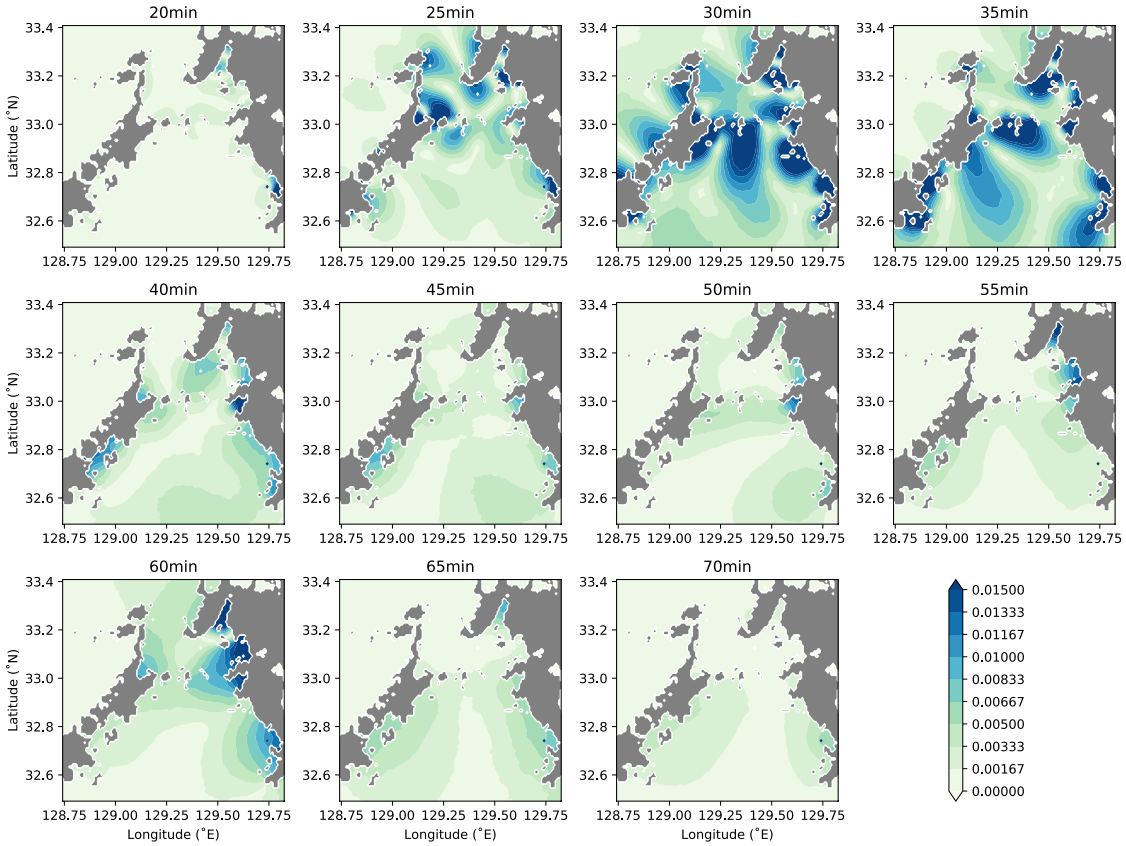


**Figure 2.17** Distributions of maximum wave heights (m) formed by periodic driving forces at the entrance of Nagasaki Bay with periods of 20-70 min with the islands located west and north of Nagasaki Bay.

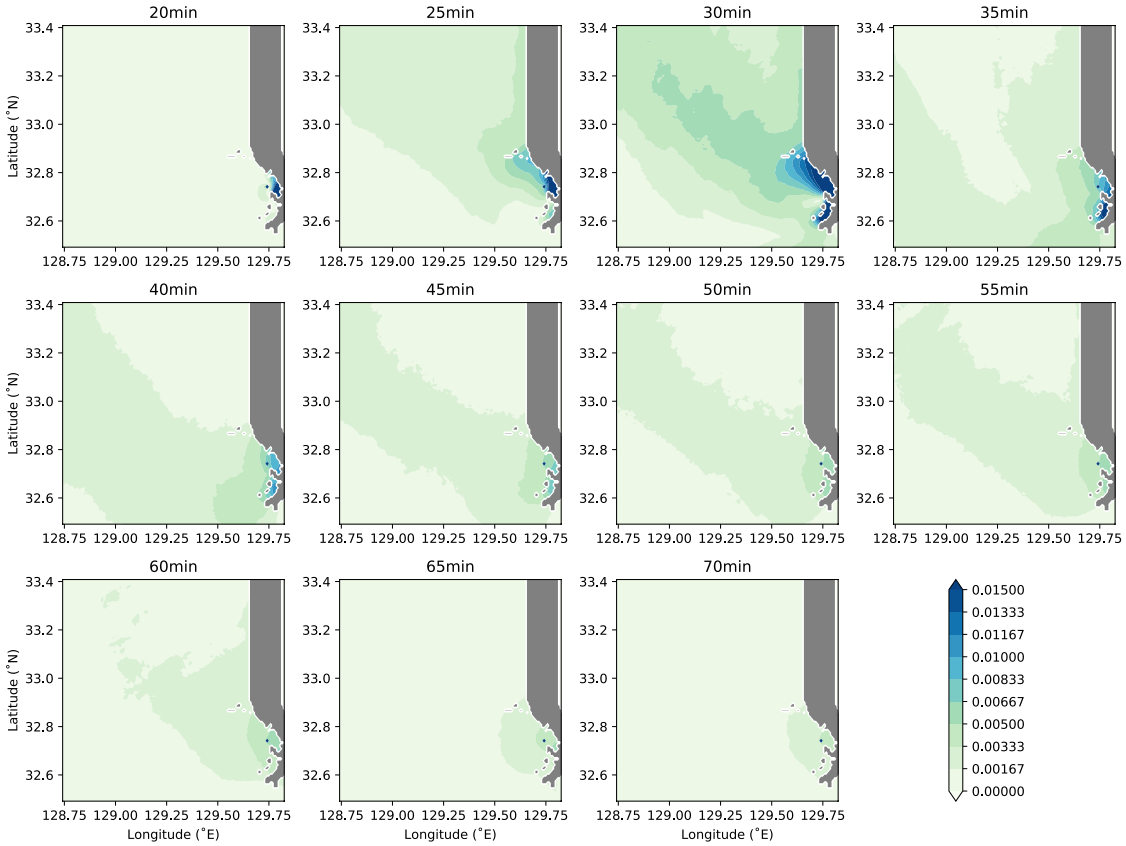


**Figure 2.18** Distributions of maximum wave heights (m) formed by periodic driving forces without the islands located west and north of Nagasaki Bay.

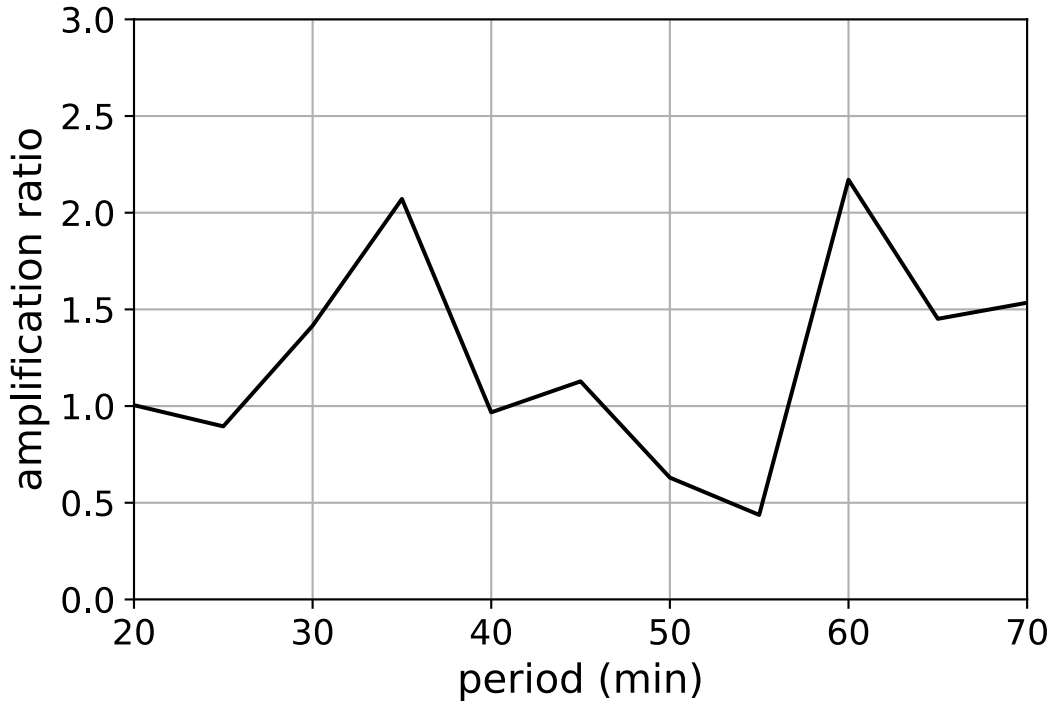


**Figure 2.19** The ratio of maximum amplitude of sea level oscillations near Nagasaki Bay formed by periodic driving forces with periods of 20-70 min with the islands located west and north of Nagasaki Bay to that without the islands located west and north of Nagasaki Bay.

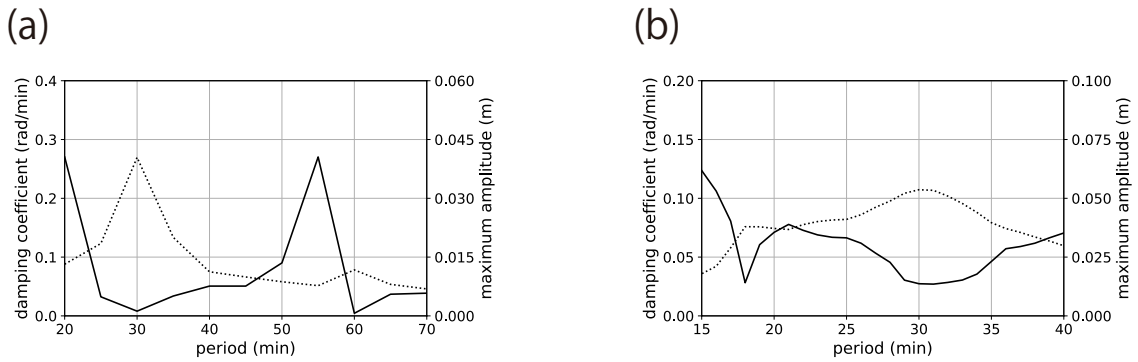


**Figure 2.20** Computed damping coefficient (solid line) and maximum sea level oscillation's amplitude (broken line), as a function of period (min) near Nagasaki Bay (a). Computed damping coefficient (solid line) and maximum sea level oscillation's amplitude (broken line), as a function of period (min) at the Nagasaki tide station (b).

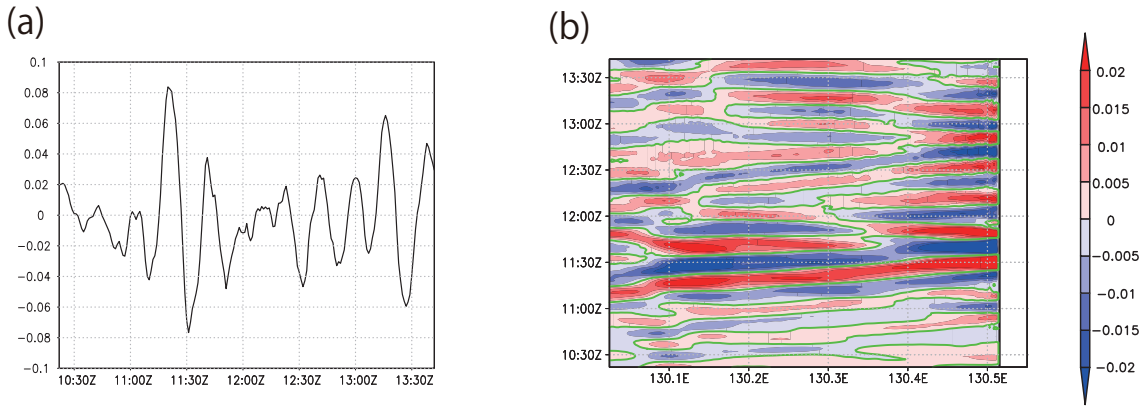


**Figure 2.21** Simulated sea level variations (m) at the entrance of Makurazaki Bay, around 130.3°E, (a). Band-pass filtered simulated sea level (m) on a transect (drawn as a green line in Figure 2.9(a)) along the coast line around Makurazaki Bay as a function of time (b). From Fukuzawa and Hibiya (2019).

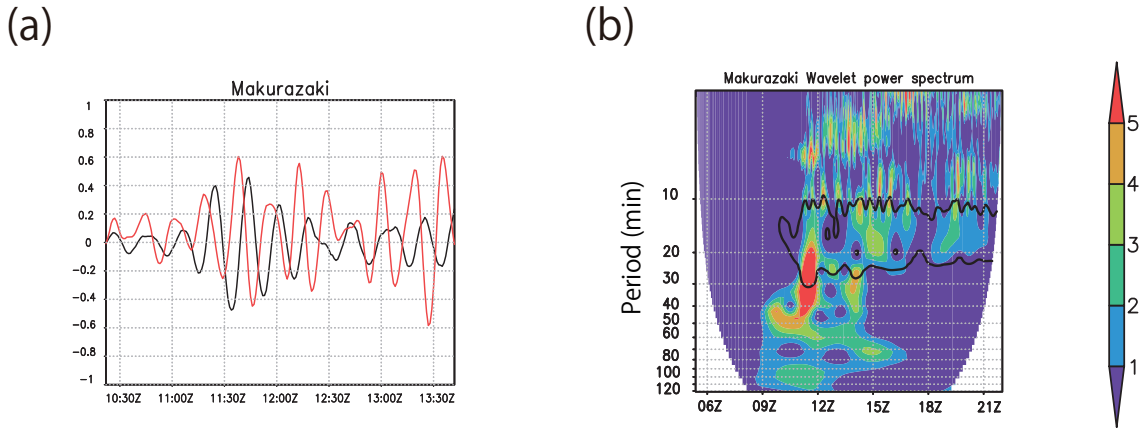


**Figure 2.22** Observed (red solid line) and calculated without Cape Kaimondake (black line) time series of sea level (m) at the Makurazaki tide station (a). Wavelet spectrum (using the Morlet wavelet) of sea level during numerical calculation without Cape Kaimondake at the Makurazaki tide station (b). Color shading represents the wavelet power. Solid black line contours enclose regions of greater than 95 % confidence level for a red noise process. From Fukuzawa and Hibiya (2019).

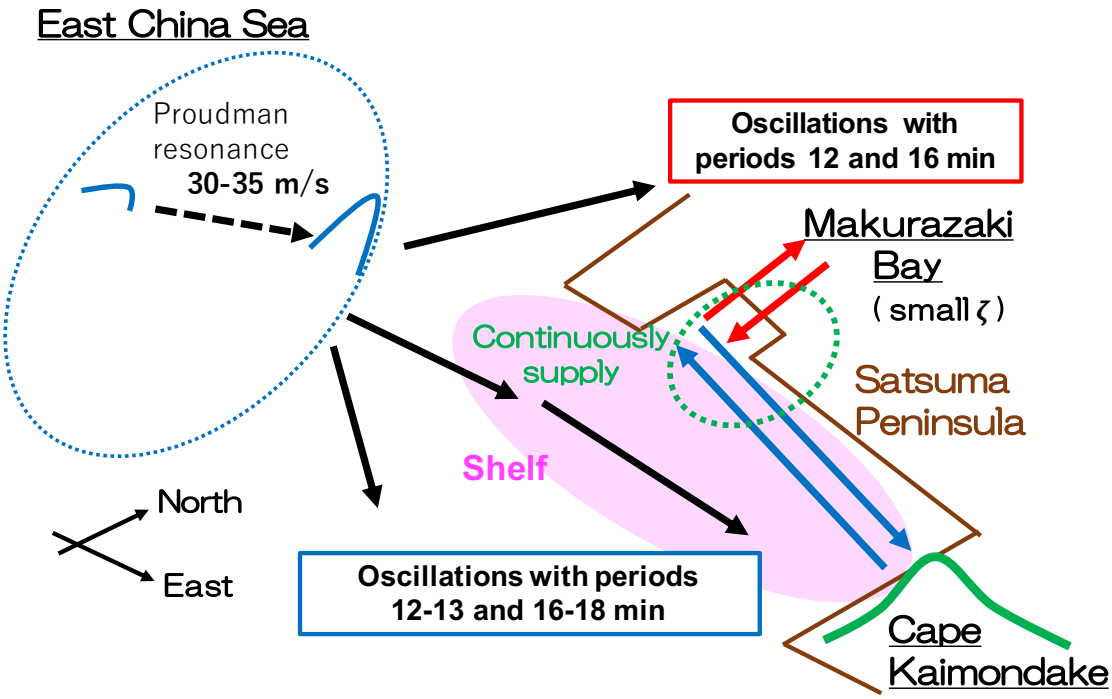


**Figure 2.35** A sketch of the amplification mechanism of the meteo-tsunami in Makurazaki Bay. The Proudman resonance (first resonance) worked over the continental shelf in the East China Sea and the resonant connection between shelf oscillations and bay oscillations are formed.

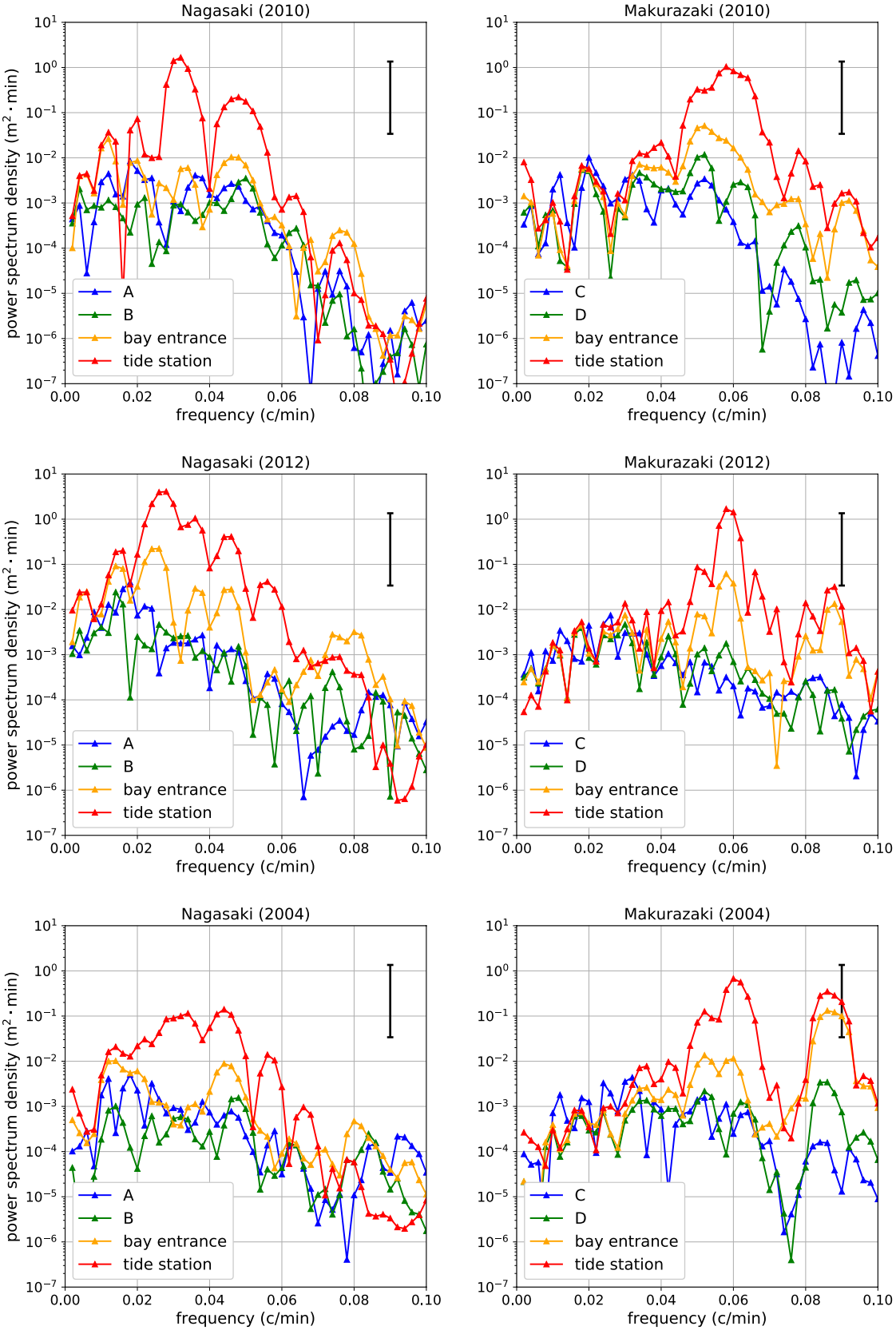
Nagasaki (2010)
Makurazaki (2010)
Nagasaki (2012)
Makurazaki (2012)
Nagasaki (2004)
Makurazaki (2004)
power spectrum density (m² · min)
frequency (c/min)
A
B
C
D
bay entrance
tide station

**Figure 2.36** Power spectra of simulated sea level variations caused by the 2010 (2012; 2004) meteo-tsunami at Locations A and B (see Figure 2.1), the location near the bay entrance of Nagasaki Bay and the Nagasaki tide station, and at Locations C and D, the location near the bay entrance of Makurazaki Bay and the Makurazaki tide station in the top (middle; bottom) panels. The error black bars show the 95% confidence interval.

## Tables

**Table 2.1**

Indexes to quantify the accuracy of the model of the 2010 meteo-tsunamis which are calculated using data during the same period of Figure 2.4.

| | The 2010 meteo-tsunami | |
|---|---|---|
| Station | Nagasaki | Makurazaki |
| Simulated maximum amplitude (m) | 0.57 | 0.73 |
| Observed maximum amplitude (m) | 0.57 | 0.62 |
| Error of maximum amplitude (%) | 0.80 | 18 |
| Lag-correlation of amplitude time series | 0.64 | 0.83 |
| Time lag (min) | 7 | 4 |
| RMSE of amplitude time series (m) | 0.13 | 0.11 |
| Simulated standard deviation of sea level variations (m) | 0.25 | 0.24 |
| Observed standard deviation of sea level variations (m) | 0.28 | 0.24 |

# Chapter 3

# A possible forecasting system of meteo-tsunamis

本節については、５年以内に雑誌等で刊行予定のため、非公開。

# Chapter 4

# General conclusions

In this thesis, the amplification mechanism of meteo-tsunamis originating west of Kyushu Island is examined, especially focusing on the transient response, and their possible forecasting system based on early detection of oceanic waves is proposed. This chapter summarizes the main results of this thesis (Figure 4.1) and discusses possible impacts of this thesis as well as future directions.

## 4.1 Summary

In chapter 2, we have carried out a numerical simulation to investigate the universal amplification mechanism of a typical meteo-tsunami in the winter of 2010 that caused large sea level oscillations along the west coast of Kyushu Island, in particular in Nagasaki Bay and Makurazaki Bay. It has been motivated by the fact that the universal amplification mechanism of meteo-tsunamis was not clarified.

It has been shown that the shelf region surrounded by the northwestern coast of Kyushu Island and the Goto Islands (Goto Nada) plays an important role by creating oceanic waves with periods of 20–40 min that are resonant with eigen-oscillation in Nagasaki Bay, consistent with Hibiya and Kajiura (1982). Additional numerical experiments driven by ideal periodic forcing using two types of topography have shown that oceanic waves repeat eastward–westward reflections on the continental shelf surrounded by the northwestern coast of Kyushu Island and the Goto Islands, gradually creating eigen-oscillations, which can effectively supply resonant oceanic waves with periods of around 30 min to Nagasaki Bay.

In Makurazaki Bay, on the other hand, significant spectral peaks have been found at periods of 10–25 min during the amplification phase of sea level oscillations, indicating that oceanic waves with these periods are strongly related to the meteo-tsunami. Additional numerical experiments focusing on the continental shelf near Makurazaki Bay have shown that edge waves repeat eastward–westward reflections on the elongated shelf between Cape Kaimondake and Cape Noma, gradually creating lateral eigen-oscillations, which can supply resonant oceanic waves with periods of 12 and 16 min to Makurazaki Bay. Because the damping coefficient of sea level oscillations in Makurazaki Bay is small, the resonant amplification of sea level oscillations occurs when the resonant oceanic waves are continuously supplied from the continental shelf to Makurazaki Bay.

It has been shown that the amplification mechanism of meteo-tsunamis in

Nagasaki Bay and Makurazaki Bay mentioned above also worked in the meteo-tsunamis in the winter of 2012 and 2004.

In chapter 3, a forecasting system of meteo-tsunamis originating west of Kyushu Island has been proposed based on the observation of sea level variations using a sea level instrument arrayed at Meshima Island, the eastern end of the East China Sea, and commercial airplanes traveling east–west over the East China Sea; there exist two regular routes, the northern route passing over the Goto Islands and the southern route passing over the Satsuma Peninsula. The workflow of the forecasting system of meteo-tsunamis is as follows. Firstly, sea level heights are continuously monitored by the sea level instrument deployed at the station in Meshima Island and by commercial airplanes traveling on the northern and southern paths. Secondly, when two or more airplanes detect significant sea level heights, we combine the information about the locations of the significant sea level heights to judge whether or not it is an oceanic wave propagating eastward. Thirdly, we estimate the characteristics of the oceanic wave such as the propagation direction and the wave period. Fourthly, forecasts of sea level oscillations are carried out for the tide stations in Nagasaki Bay and Makurazaki Bay and the stations in Meshima Island and off the Satsuma Peninsula. When the data of oceanic wave such as its amplitude, arrival time, and period are available at the station in Meshima Island, the forecasts consistent with the observed data are chosen. In addition, when the oceanic wave is observed near the coast of the Satsuma Peninsula by airplanes traveling on the southern route, forecasts consistent with the observation are chosen taking into account its amplitude. Finally, continuous monitoring of significant oceanic waves on the continental shelf in the East China Sea is carried out throughout the damping timescale of sea level oscillations in Nagasaki Bay and Makurazaki Bay because the amplitude of sea level oscillations will grow if an oceanic wave is incident while the oscillation continues. In order to check the validity of this forecasting system, it has been applied to the 2010 meteo-tsunami to show the forecasts are consistent with the answers.

We note that the numerical simulation of the generation and propagation of the atmospheric disturbance is desirable in the future, since the results of the studies on meteo-tsunamis are subject to the uncertainty of the temporal and spatial structure of the atmospheric disturbance. Such numerical simulations are also useful to clarify the

relationship between the synoptic atmospheric pattern and small-scale atmospheric disturbances, which will help us to construct the prediction system for meteo-tsunamis originating west of Kyushu Island. As for the forecasting system, the effects of observation error on the forecasts should be considered in the future. The observation error of sea level heights has an effect on the estimation of the amplitude, the propagation direction, and the period of an oceanic wave. Therefore, it should be examined through an observation campaign using airborne altimetry radar focusing on small-scale structure of 10–100 km.

In summary, this thesis has shown that the resonant coupling of eigen-oscillations between the bay and its offshore shelf occurs resulting in large meteo-tsunamis in Nagasaki Bay and Makurazaki Bay, with a special attention to the transient response. Furthermore, a possible forecasting system of meteo-tsunamis using airborne altimetry radar has been proposed.

## 4.2 Impacts of this thesis and future directions

The importance of understanding the transient response of a bay to an incident oceanic wave is emphasized in this thesis, which has been overlooked in the previous studies. Based on the fact that the amplitude of sea level variations in meteo-tsunamis grows gradually, the understanding of the transient response is necessary to predict when the amplitude attains its maximum and how long the excited oscillation continues. Studies on a system which continuously supplies oceanic waves to a bay should also be carried out at other areas in the world's oceans where large meteo-tsunamis are frequently observed; they must promote our understanding of meteo-tsunamis.

This thesis also contributes to our understanding of atmospheric disturbances causing meteo-tsunamis, for example, some small-scale meteorological phenomena with rapid pressure and/or wind stress changes. As mentioned already, further effort is necessary to reproduce such small-scale features by taking into account uncertainties of initial conditions, space-time resolution, and some parameterizations (e.g. Horvath and Vilibić, 2014). On the other hand, focusing on the oceanic response, oceanic waves which come from the East China Sea to the coast in Kyushu Island can be calculated inversely using observed sea level variations at tide stations based on the understanding of the amplification mechanism, in particular, a system supplying oceanic waves to a bay.

Although the implementation of the inversion scheme from the oceanic response to the atmospheric forcing is required, it will be useful to check the reproducibility of atmospheric simulations. Since some studies using numerical simulation based on coupled atmosphere-ocean models did not analyze the differences between the simulated and observed data, such a mutual feedback between oceanic and atmospheric models have to be carried out focusing on each meteo-tsunami case.

At the same time, statistical studies on the atmospheric phenomena causing meteo-tsunamis are also important; the seasonality of meteo-tsunamis in the individual area should be considered (e.g. Bechle et al., 2015). In addition, interannual variability of meteo-tsunamis is a possible research topic: it is pointed out that the interannual variability of occurrence of meteo-tsunamis in the northeastern Gulf of Mexico is related to El Niño–Southern Oscillation (Olabarrieta et al., 2017). Furthermore, if the long-term trend of sea level rise related to global warming is taken into account, it will increase the flood risk and might change the periods of eigen-modes in bays, in particular in shallow bays: it might change the existing resonant couplings of eigen-oscillations.

The importance of understanding meteo-tsunamis is emphasized based on their influence on ecosystem. Basterretxea et al. (2011) explained that a seiche, sea level oscillation in a bay or harbor, induced release of nutrients from the sediment causing ecosystem response at Peguera, located on the northwestern coast of Santa Ponça Bay, Mallorca, Balearic Islands, the Mediterranean Sea. Actually, the effect of meteo-tsunamis on bottom shear stress in the estuaries in the Great Lakes were examined in some detail (Linares et al., 2018). The fact that a meteo-tsunami stimulates the biological environment in a bay implies that the differences of biological environments are partially explained in terms of the differences of amplification mechanism of meteo-tsunamis in coastal areas. A physical relationship between meteo-tsunamis and biological environment should be examined and quantified in other areas all over the world.

Finally, the verification of the forecasting system of meteo-tsunamis will contribute to the construction of the forecasting system of seismic tsunamis. Because it is difficult to predict the occurrence of seismic tsunamis, operational systems forecasting seismic tsunami waves mainly depend on some observation systems such as seismometers, strain meters, seismic intensity meters, tide gauges, GPS buoys, and

offshore-water-pressure gauges. Recent studies pointed out that it is useful to make use of the offshore observation of sea level heights using GPS buoys and bottom pressure gauges to improve estimation of the initial sea surface displacement, leading to the improvement of tsunami forecast (eg. Hossen et al., 2015, 2017; Mulia et al., 2018). Indeed, two big observation networks consisting of seismometers and bottom pressure gauges are distributed around Japan which are expected to contribute early forecast of tsunamis: Seafloor Observation Network for Earthquakes and Tsunamis along the Japan Trench (S-net) and The Dense Ocean floor Network System for Earthquakes and Tsunamis (DONET). However, the operation of such offshore observation systems costs much. Therefore, it is not realistic to distribute such observation networks to all over the world, although seismic tsunamis have attacked all over the world. Based on the above circumstances, observation of sea level heights by commercial airplanes is expected to cover the blank areas using existing facilities. The verification of the forecasting system of seismic tsunamis based on airplanes' observation is not easy to implement using the realistic tsunami data due to the low frequency of occurrences of seismic tsunamis. However, it would be possible to implement using the meteo-tsunamis data because meteo-tsunamis occur more frequently than large seismic tsunamis at certain areas. Increasing the reliability of forecasting system of meteo-tsunamis will contribute to the development of the accuracy of the system forecasting seismic tsunamis in the world.

## Figures

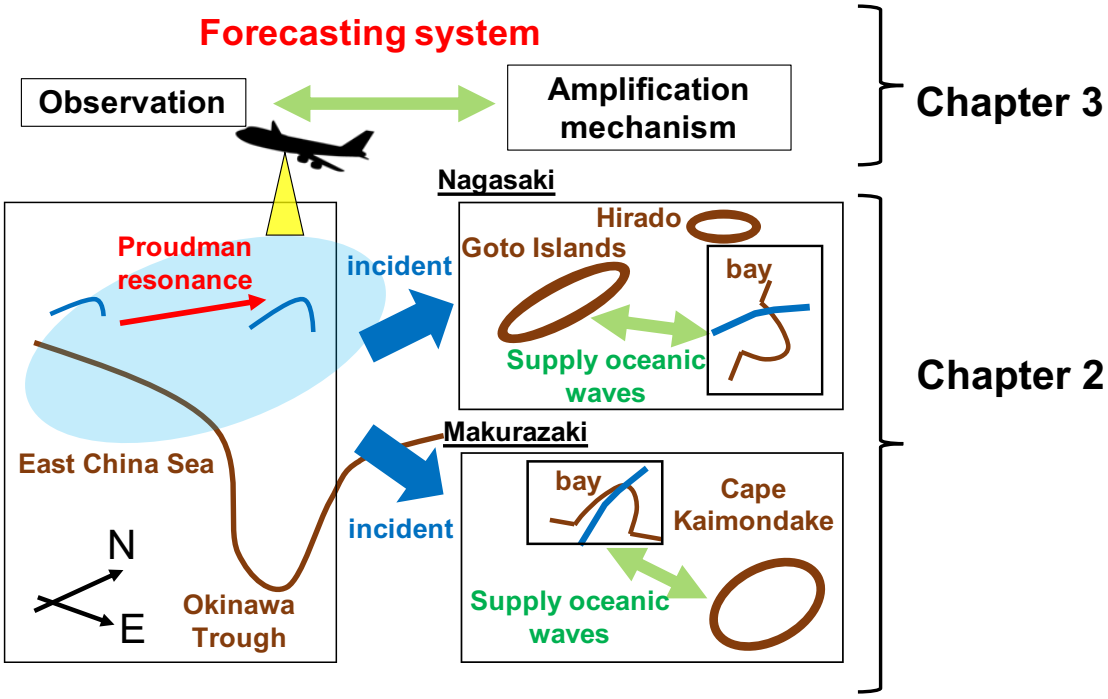


**Figure 4.1** A sketch of the summary of this thesis.

# Appendix

## A.1 The estimation of the propagation speed and propagation direction

The estimates of the propagation speed and direction of an atmospheric disturbance can be conducted using the maximum likelihood estimation method (Šepić et al., 2009). Let $\Delta t_i$ be the estimated difference between arrival times of the atmospheric pressure disturbance at meteorological stations with a distance, $\delta_i$. with the angle, $\gamma_i$ counterclockwise from the east. The optimal propagation speed, $v$, and propagation direction, $\gamma$, of the atmospheric pressure disturbance can be obtained by minimizing the following function,

$$f(v,\gamma) = \sum_{i=1}^{n} (\Delta t_i - \Delta t_i')^2 = \sum_{i=1}^{n} (\frac{\delta_i \cos(\gamma_i - \gamma)}{v} - \Delta t_i')^2 \qquad \text{(A-1-1)}$$

where $\Delta t_i'$ is observed difference between arrival times and $n$ is the number of station pairs.

The distribution of (A-1-1) calculated using observed values when the 2010 (2012, 2004) meteo-tsunami occurred is shown in Figure A.1.1 (A.1.2, A.1.3). The assumed propagation speed and propagation direction in Section 2.2 (2.3, 2.4) is in the area close to the minimum point.

## A.2 An index to quantify the accuracy of the meteo-tsunami models

In the previous studies on meteo-tsunamis, maximum and minimum wave heights are used as indexes of the validity of the numerical model (e.g. Orlić et al., 2010; Vilibić et al., 2010). Although a similar index which is calculated using the observed and simulated maximum amplitude of an oceanic wave is adopted to check the validity of numerical simulation of seismic tsunamis (e.g. Tsushima et al., 2012), it is not an index

to explain whether or not the model reproduce the growth of the sea level oscillations; it is insufficient to represent one of special characteristics of meteo-tsunamis being amplified gradually in a bay.

In order to discuss the accuracy of the meteo-tsunami models, we should use an index which explains the variation of the sea level oscillations. An index is defined as the lag correlation coefficient of the variations of the sea level oscillations' amplitude, $A_o(t)$ and $A_s(t)$, which are obtained by applying the Hilbert transform method to observed data and simulated data. Since both $A_o(t)$ and $A_s(t)$ take values greater than or equal to 0, their correlation coefficient represent the variation of their amplitudes without the oscillating components. In addition, another index expressing the differences between $A_o(t)$ and $A_s(t)$ is defined as the standard deviation.

## A.3 The eigenvalue problem

For the linearized, non-rotating, non-viscous shallow water equations of motion and continuity (2-1, 2-2 and 2-3), a solution of periodic waves, $\eta\, e^{i\omega t}$, satisfies the following equation,

$$\frac{\partial}{\partial x}\left(H\frac{\partial \eta}{\partial x}\right)+\frac{\partial}{\partial y}\left(H\frac{\partial \eta}{\partial y}\right)+\frac{\omega^2}{g}\eta=0 \qquad \text{(A-3-1)}$$

where $\omega$ is the frequency (Loomis, 1996).

Converting this equation to a difference equation by the central difference formula, $N$ independent equations are obtained where $N$ is the total number of grid points. The equation at the grid point $(i, j)$ is

$$l^2\omega^2\eta_{i,j}=A_e\eta_{i+1,j}+A_w\eta_{i-1,j}+A_n\eta_{i,j+1}+A_s\eta_{i,j-1}+A_c\eta_{i,j} \qquad \text{(A-3-2)}$$

$$A_e=g\frac{H_{i+1,j}+H_{i,j}}{2}$$

$$A_w=g\frac{H_{i-1,j}+H_{i,j}}{2}$$

$$A_n=g\frac{H_{i,j+1}+H_{i,j}}{2}$$

$$A_s=g\frac{H_{i,j-1}+H_{i,j}}{2}$$

$$A_c=-(A_e+A_w+A_n+A_s)$$

with $l$ the grid interval. We assume nodal lines at the south and west boundaries of the

calculation domain, $\eta_{i,1} = -\eta_{i,2}$ and $\eta_{1,j} = -\eta_{2,j}$, respectively. If the grid $(i, j)$ is located on land, the sea depth and the coefficient of $\eta_{i,j}$ are both set to zero. The eigenvalue problem is solved using the LAPACK Library, "DGEEV" function.

## Figures

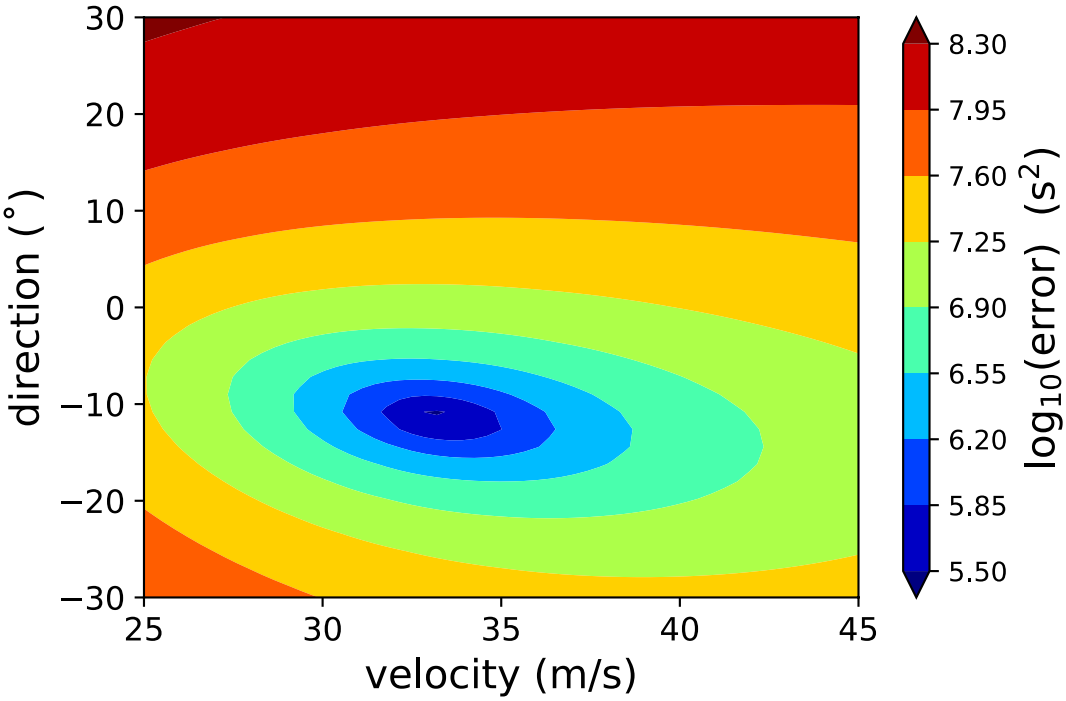


**Figure A.1.1** The distribution of the error ($s^2$) in the estimation of propagation speed (horizontal axis) and propagation direction (vertical axis) using the meteorological data obtained when the 2010 meteo-tsunami occurred.

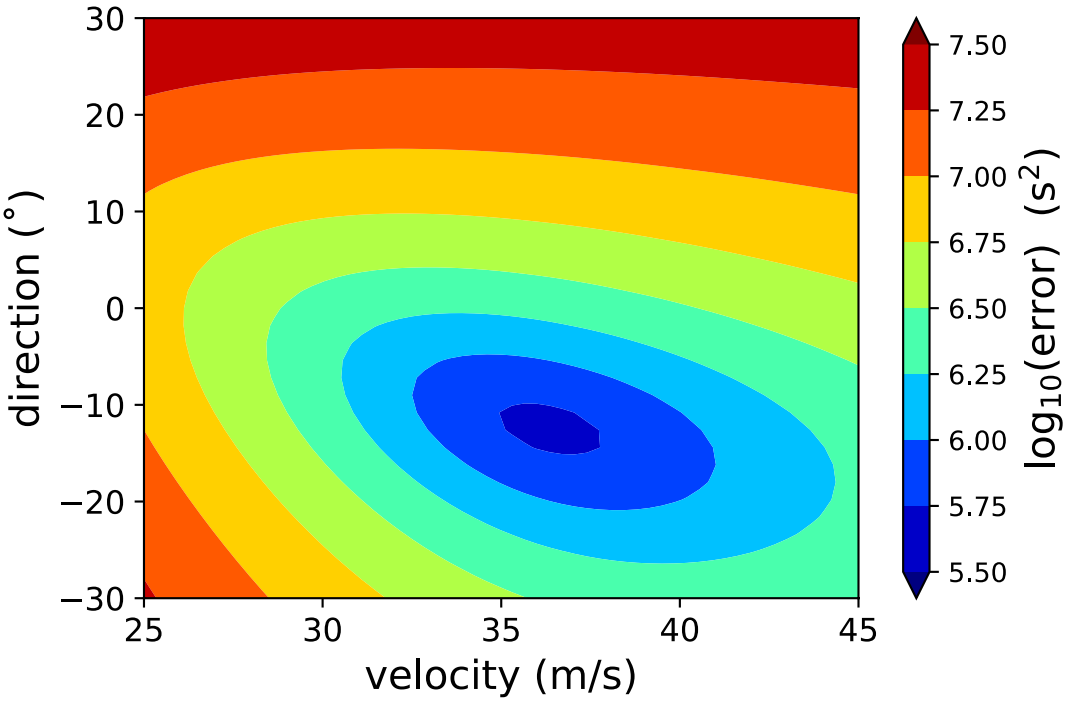


**Figure A.1.2** As in Figure A.1.2, but for the 2012 meteo-tsunami.

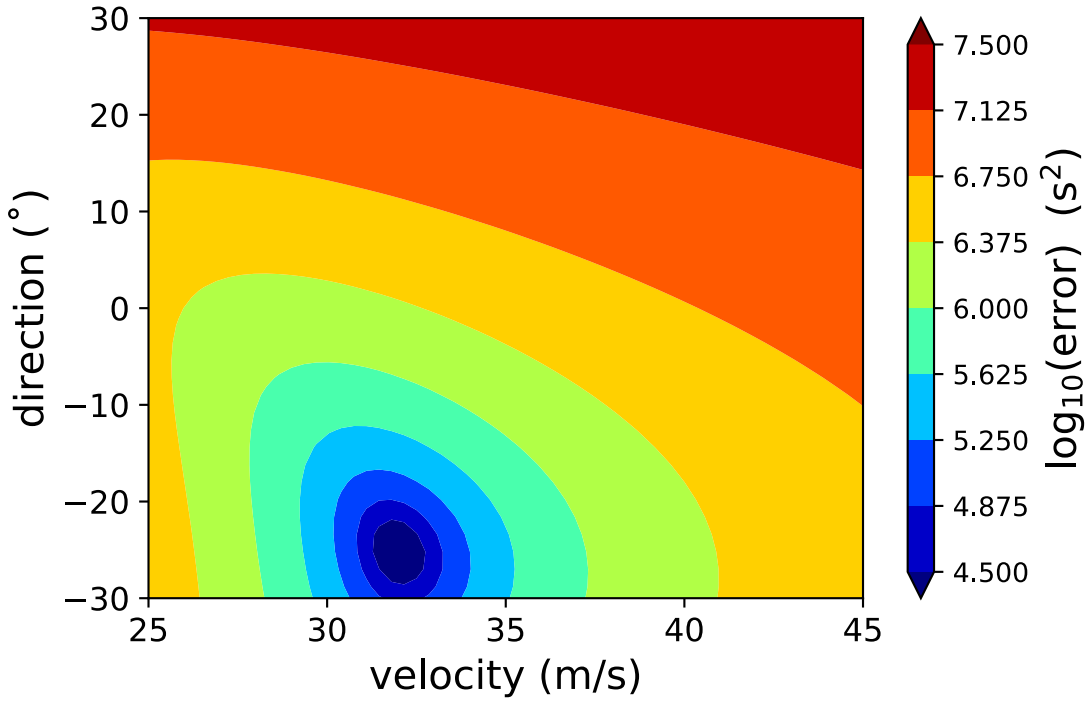


**Figure A.1.3** As in Figure A.1.1, but for the 2004 meteo-tsunami.

# Acknowledgements

First and foremost, I would like to express my sincere gratitude to the supervisor, Prof. Toshiyuki Hibiya for his sincere support of my Ph.D. studies and related research. This work would not have been possible without his continuous support.

I would like to thank the members of my dissertation committee, Profs. Hiroyasu Hasumi, Yukio Masumoto, Tomoki Tozuka, and Hiroaki Miura for their time and many valuable comments. I am grateful very helpful members and ex-members of the Atmosphere and Oceanic Science Group, the University of Tokyo. Special thanks to Drs. Yoshihiro Niwa, Takahiro Endoh, Yuki Tanaka, Taira Nagai, Takashi Ijichi, Yohei Onuki, Daisuke Inazu, Tomoyuki Hirobe for their helpful suggestions and encouragement. This study has been benefited from the discussions with Drs. Hiroshi Niino, Kaoru Sato, Makoto Koike, Naoki Hirose, Hidenori Aiki, Satoshi Osafune, Takahiro Toyoda, Kei Sakamoto, Shinya Kouketsu, Takashi Sakamoto, Kazuaki Nishii, Tekeya Kinoshita, Kenji Tanaka, and Junshi Ito. In addition, I would like to thank Drs. Richard Thomson, Alexander Rabinovich, Isaac Fine, Roy Hourston and Brenda Burd for their hospitality and warm guidance during my internship at Institute of Ocean Sciences, Canada. Thanks also to Shun Ohishi, Ryosuke Shibuya, Shota Katsura, Masatoshi Miyamoto, Yoko Yamagami, Hajime Ishii, Tamaki Suematsu, Chiarui Ong, Soichiro Hirano, Ryosuke Yasui, Shoichiro Kido, Shion Sekizawa, Daisuke Takasuka, Shuhei Matsugishi, Anne Takahashi, Atsushi Yoshida, Yuichi Minamihara, Takuro Matsuta, Marvin Seow Xiang Ce, Emiri Kobori, Dai Koshin, Kazumichi Murata, Takuya Jinno, Aiqi Zhang, Takahiro Yanagimachi, Natsumi Tanuma, Takahiro Kusumi, Hidehiro Kusunoki, Mai Nakazato, Yoo-Jun Kim, Rika Yoshiyama and all past and present members of Atmospheric and Oceanic Science Group and faculty members of Department of Earth and Planetary Science. Also, I give a special thanks to all friends, particularly Masanori Iwamoto, Osamu Sandanbata, Reina Hikida, Ryo Yamamoto, Yusuke Ushijima, and Yasushi

Fujiwara.

I would like to acknowledge the funding sources. I was supported by Leading Graduate Course for Frontiers of Mathematical Sciences and Physics (FMSP) and by the Sasakawa Scientific Research Grant from The Japan Science Society.

Part of numerical calculations were carried out on Oakforest-PACS system in the Information Technology Center, the University of Tokyo. Some figures were produced by The Grid Analysis and Display System (GrADS).

Finally, I wish to thank my family for their support and encouragement.

# References

Amante, C., & Eakins, B. W. (2009). ETOPO1 1 Arc-Minute Global Relief Model: Procedures, Data Sources and Analysis. *National Geophysical Data Center, NESDIS, NOAA, U.S. Dept. Commerce, Boulder, CO, USA*. https://doi.org/10.7289/V5C8276M

Asano, T., Yamashiro, T., Takeshita, A., Sakamoto, H., & Nishimura, N. (2011). Field Observation of Secondary Undulation "Abiki" in Urauchi Bay, Kami-Koshiki Island. *Journal of Japan Society of Civil Engineers, Ser. B2 (Coastal Engineering)*, *67*(2), I_176-I_180. https://doi.org/10.2208/kaigan.67.I_176

Asano, T., Yamashiro, T., Yamaguchi, D., & Kobaru, R. (2014). A Field Observation of Meteo-tsunamis Excited by Geometric Resonance on the Continental Shelf off Makurazaki Coast. *Journal of Japan Society of Civil Engineers, Ser. B2 (Coastal Engineering)*, *70*(2), I_141-I_145. https://doi.org/10.2208/kaigan.70.I_141

Basterretxea, G., Jordi, A., Garcés, E., Anglès, S., & Reñé, A. (2011). Seiches stimulate transient biogeochemical changes in a microtidal coastal ecosystem. *Marine Ecology Progress Series*, *423*, 15–28. https://doi.org/10.3354/meps08949

Bechle, A. J., & Wu, C. H. (2014). The Lake Michigan meteotsunamis of 1954 revisited. In *Meteorological Tsunamis: The U.S. East Coast and Other Coastal Regions* (pp. 155–177). Cham: Springer International Publishing. https://doi.org/10.1007/978-3-319-12712-5_9

Bechle, A. J., Kristovich, D. A. R., & Wu, C. H. (2015). Meteotsunami occurrences and causes in Lake Michigan. *Journal of Geophysical Research: Oceans*, *120*(12), 8422–8438. https://doi.org/10.1002/2015JC011317

Bellotti, G. (2007). Transient response of harbours to long waves under resonance conditions. *Coastal Engineering*, *54*(9), 680–693. https://doi.org/10.1016/j.coastaleng.2007.02.002

Belušić, D., Grisogono, B., & Klaić, Z. B. (2007). Atmospheric origin of the devastating coupled air-sea event in the east Adriatic. *Journal of Geophysical Research Atmospheres*, *112*(17), 1–14. https://doi.org/10.1029/2006JD008204

Bubalo, M., Janeković, I., & Orlić, M. (2018). Chrystal and Proudman resonances simulated with three numerical models. *Ocean Dynamics*, *68*(4–5), 497–507. https://doi.org/10.1007/s10236-018-1146-8

Carvajal, M., Contreras-López, M., Winckler, P., & Sepúlveda, I. (2017). Meteotsunamis Occurring Along the Southwest Coast of South America During an Intense Storm. *Pure and Applied Geophysics*, *174*(8), 3313–3323. https://doi.org/10.1007/s00024-017-1584-0

Drago, A. (2009). Sea level variability and the 'Milghuba' seiche oscillations in the northern coast of Malta, Central Mediterranean. *Physics and Chemistry of the Earth, Parts A/B/C*, *34*(17–18), 948–970. https://doi.org/10.1016/j.pce.2009.10.002

Endoh, T., Inazu, D., Waseda, T., & Hibiya, T. (2018). A parameter quantifying radiation damping of bay oscillations excited by incident tsunamis. *Continental Shelf Research*, *157*(April 2017), 10–19. https://doi.org/10.1016/j.csr.2018.02.007

Fukuzawa, K., & Hibiya, T. (2019). The amplification mechanism of a meteo-tsunami

originating off the western coast of Kyushu Island of Japan in the winter of 2010. *Journal of Oceanography*. https://doi.org/10.1007/s10872-019-00536-3

Goring, D. G. (2009). Meteotsunami resulting from the propagation of synoptic-scale weather systems. *Physics and Chemistry of the Earth, Parts A/B/C*, *34*(17–18), 1009–1015. https://doi.org/10.1016/j.pce.2009.10.004

Gower, J. (2007). The 26 December 2004 tsunami measured by satellite altimetry. *International Journal of Remote Sensing*, *28*(13–14), 2897–2913. https://doi.org/10.1080/01431160601094484

Greenspan, H. P. (1956). The generation of edge waves by moving pressure distributions. *Journal of Fluid Mechanics*, *1*(06), 574–592. https://doi.org/10.1017/S002211205600038X

Heidarzadeh, M., Šepić, J., Rabinovich, A., Allahyar, M., Soltanpour, A., & Tavakoli, F. (2019). Meteorological Tsunami of 19 March 2017 in the Persian Gulf: Observations and Analyses. *Pure and Applied Geophysics*, (March 2017). https://doi.org/10.1007/s00024-019-02263-8

Hibiya, T., & Kajiura, K. (1982). Origin of the Abiki phenomenon (a kind of seiche) in Nagasaki Bay. *Journal of the Oceanographical Society of Japan*, *38*(3), 172–182. https://doi.org/10.1007/BF02110288

Hirobe, T., Niwa, Y., Endoh, T., Mulia, I. E., Inazu, D., Yoshida, T., Tatehata, H., Nadai, A., Waseda, T., & Hibiya, T. (2019). Observation of sea surface height using airborne radar altimetry: a new approach for large offshore tsunami detection. *Journal of Oceanography*, *75*(6), 541–558. https://doi.org/10.1007/s10872-019-00521-w

Horvath, K., & Vilibić, I. (2014). Atmospheric mesoscale conditions during the

Boothbay meteotsunami: a numerical sensitivity study using a high-resolution mesoscale model. In *Meteorological Tsunamis: The U.S. East Coast and Other Coastal Regions* (pp. 55–74). Cham: Springer International Publishing. https://doi.org/10.1007/978-3-319-12712-5_4

Hossen, M. J., Cummins, P. R., & Satake, K. (2017). Complete Implementation of the Green's Function Based Time Reverse Imaging and Sensitivity Analysis of Reversed Time Tsunami Source Inversion. *Geophysical Research Letters*, *44*(19), 9844–9855. https://doi.org/10.1002/2017GL074528

Hossen, M. Jakir, Cummins, P. R., Roberts, S. G., & Allgeyer, S. (2015). Time Reversal Imaging of the Tsunami Source. *Pure and Applied Geophysics*, *172*(3–4), 969–984. https://doi.org/10.1007/s00024-014-1014-5

Inazu, D., Waseda, T., Hibiya, T., & Ohta, Y. (2016). Assessment of GNSS-based height data of multiple ships for measuring and forecasting great tsunamis. *Geoscience Letters*, *3*(1), 25. https://doi.org/10.1186/s40562-016-0059-y

Indika, K. W., Ranagalage, M., Wijerathne, E. M. S., & Hettiarachchi, S. S. L. (2017). Determination of the Potential of Meteotsunami in the West Coast of Sri Lanka. *International Journal of New Technology and Research*, *3*(10), 1–3. Retrieved from https://www.ijntr.org/download_data/IJNTR03100003.pdf

Jansa, A., Monserrat, S., & Gomis, D. (2007). The rissaga of 15 June 2006 in Ciutadella (Menorca), a meteorological tsunami. *Advances in Geosciences*, *12*, 1–4. https://doi.org/10.5194/adgeo-12-1-2007

de Jong, M. P. C., & Battjes, J. A. (2004). Low-frequency sea waves generated by atmospheric convection cells. *Journal of Geophysical Research*, *109*(C1), C01011. https://doi.org/10.1029/2003JC001931

Kim, H., Kim, M.-S., Kim, Y.-K., Yoo, S.-H., & Lee, H.-J. (2017). Numerical Weather Prediction for Mitigating the Fatal Loss by the Meteo-tsunami Incidence on the West Coast of Korean Peninsula. *Journal of Coastal Research*, *79*, 119–123. https://doi.org/10.2112/SI79-025.1

Kim, M.-S., Kim, H., Eom, H.-M., Yoo, S.-H., & Woo, S.-B. (2019). Occurrence of Hazardous Meteotsunamis Coupled with Pressure Disturbance Traveling in the Yellow Sea, Korea. *Journal of Coastal Research*, *91*(sp1), 71. https://doi.org/10.2112/SI91-015.1

LeBlond, P., & Mysak, L. (1981). *Waves in the Ocean*. Elsevier.

Ličer, M., Mourre, B., Troupin, C., Krietemeyer, A., Jansá, A., & Tintoré, J. (2017). Numerical study of Balearic meteotsunami generation and propagation under synthetic gravity wave forcing. *Ocean Modelling*, *111*, 38–45. https://doi.org/10.1016/j.ocemod.2017.02.001

Linares, Á., Bechle, A. J., & Wu, C. H. (2016). Characterization and assessment of the meteotsunami hazard in northern Lake Michigan. *Journal of Geophysical Research: Oceans*, *121*(9), 7141–7158. https://doi.org/10.1002/2016JC011979

Linares, Á., Wu, C. H., Anderson, E. J., & Chu, P. Y. (2018). Role of Meteorologically Induced Water Level Oscillations on Bottom Shear Stress in Freshwater Estuaries in the Great Lakes. *Journal of Geophysical Research: Oceans*, *123*(7), 4970–4987. https://doi.org/10.1029/2017JC013741

Lindzen, R. S., & Tung, K.-K. (1976). Banded Convective Activity and Ducted Gravity Waves. *Monthly Weather Review*, *104*(12), 1602–1617. https://doi.org/10.1175/1520-0493(1976)104<1602:BCAADG>2.0.CO;2

Lindzen, R. S. (1974). Wave-CISK in the Tropics. *Journal of the Atmospheric Sciences*,

*31*(1), 156–179. https://doi.org/10.1175/1520-0469(1974)031<0156:WCITT>2.0.CO;2

Loomis, H. (1996). Some numerical hydrodynamics for Hilo Harbor. *Institute of Geophysics, University of Hawaii*, *HIG-66-7*.

Mehra, P., Prabhudesai, R. G., Joseph, A., Kumar, V., Agarvadekar, Y., Luis, R., & Viegas, B. (2012). A study of meteorologically and seismically induced water level and water temperature oscillations in an estuary located on the west coast of India (Arabian Sea). *Natural Hazards and Earth System Science*, *12*(5), 1607–1620. https://doi.org/10.5194/nhess-12-1607-2012

Miles, J., & Munk, W. (1961). Harbor paradox. *Journal of the Waterways and Harbors Division Proceedings of the American Society of Civil Engineers*, *87.3*, 111–132.

Monserrat, S., & Thorpe, A. J. (1996). Use of Ducting Theory in an Observed Case of Gravity Waves. *Journal of the Atmospheric Sciences*. https://doi.org/10.1175/1520-0469(1996)053<1724:UODTIA>2.0.CO;2

Monserrat, S., Vilibić, I., & Rabinovich, A. B. (2006). Meteotsunamis: Atmospherically induced destructive ocean waves in the tsunami frequency band. *Nat. Hazards Earth Syst. Sci.*, *6*, 1035–1051. https://doi.org/10.5194/nhess-6-1035-2006

Mulia, I. E., Gusman, A. R., Jakir Hossen, M., & Satake, K. (2018). Adaptive Tsunami Source Inversion Using Optimizations and the Reciprocity Principle. *Journal of Geophysical Research: Solid Earth*, 2018JB016439. https://doi.org/10.1029/2018JB016439

Oey, L.-Y., & Chen, P. (1992). A nested-grid ocean model: With application to the simulation of meanders and eddies in the Norwegian Coastal Current. *Journal of Geophysical Research*, *97*(C12), 20063. https://doi.org/10.1029/92JC01991

Okal, E. A., Visser, J. N. J., & de Beer, C. H. (2014). The Dwarskersbos, South Africa local tsunami of August 27, 1969: field survey and simulation as a meteorological event. In *Meteorological Tsunamis: The U.S. East Coast and Other Coastal Regions* (pp. 251–268). Cham: Springer International Publishing. https://doi.org/10.1007/978-3-319-12712-5_14

Olabarrieta, M., Valle-Levinson, A., Martinez, C. J., Pattiaratchi, C., & Shi, L. (2017). Meteotsunamis in the northeastern Gulf of Mexico and their possible link to El Niño Southern Oscillation. *Natural Hazards*, *88*(3), 1325–1346. https://doi.org/10.1007/s11069-017-2922-3

Orlić, M. (1980). About a possible occurrence of the Proudman resonance in the Adriatic. *Thalassia Jugosl.*, *61*(1), 79–88.

Orlić, M., Belušić, D., Janeković, I., & Pasarić, M. (2010). Fresh evidence relating the great Adriatic surge of 21 June 1978 to mesoscale atmospheric forcing. *Journal of Geophysical Research: Oceans*, *115*(6), 1–20. https://doi.org/10.1029/2009JC005777

Pasquet, S., & Vilibić, I. (2013). Shelf edge reflection of atmospherically generated long ocean waves along the central U.S. East Coast. *Continental Shelf Research*, *66*, 1–8. https://doi.org/10.1016/j.csr.2013.06.007

Pattiaratchi, C., & Wijeratne, E. M. S. (2015). Observations of meteorological tsunamis along the south-west Australian coast. *Meteorological Tsunamis: The U.S. East Coast and Other Coastal Regions*, 281–303. https://doi.org/10.1007/978-3-319-12712-5_16

Pattiaratchi, C. B., & Wijeratne, E. M. S. (2015). Are meteotsunamis an underrated hazard? *Philosophical Transactions of the Royal Society A: Mathematical,*

*Physical and Engineering Sciences*, *373*(2053). https://doi.org/10.1098/rsta.2014.0377

Pellikka, H., Rauhala, J., Kahma, K. K., Stipa, T., Boman, H., & Kangas, A. (2015). Recent observations of meteotsunamis on the Finnish coast. *Meteorological Tsunamis: The U.S. East Coast and Other Coastal Regions*, 197–215. https://doi.org/10.1007/978-3-319-12712-5_11

Perez, I., & Walter, D. (2017). Spectral variability in high frequency in sea level and atmospheric pressure on Buenos Aires Coast, Argentina. *Brazilian Journal of Oceanography*, *65*(1), 69–78. https://doi.org/10.1590/s1679-87592017130506501

Proudman, J. (1929). The Effects on the Sea of Changes in Atmospheric Pressure. *Geophysical Journal International*, *2*(4), 197–209. https://doi.org/10.1111/j.1365-246X.1929.tb05408.x

Rabinovich, A. B. (2009). Seiches and Harbour Oscillations. *Handbook of Coastal and Ocean Engineering*, 193–236. https://doi.org/10.1142/9789812819307_0009

Rabinovich, A. B. (2019). Twenty-Seven Years of Progress in the Science of Meteorological Tsunamis Following the 1992 Daytona Beach Event. *Pure and Applied Geophysics*. https://doi.org/10.1007/s00024-019-02349-3

Šepić, J., Vilibić, I., & Belušić, D. (2009). Source of the 2007 Ist meteotsunami (Adriatic Sea). *Journal of Geophysical Research*, *114*(C3), C03016. https://doi.org/10.1029/2008JC005092

Šepić, J., Vilibić, I., & Strelec Mahović, N. (2012). Northern Adriatic meteorological tsunamis: Observations, link to the atmosphere, and predictability. *Journal of Geophysical Research: Oceans*, *117*(C2). https://doi.org/10.1029/2011JC007608

Šepić, J., Međugorac, I., Janeković, I., Dunić, N., & Vilibić, I. (2016). Multi-

Meteotsunami Event in the Adriatic Sea Generated by Atmospheric Disturbances of 25–26 June 2014. *Pure and Applied Geophysics*. https://doi.org/10.1007/s00024-016-1249-4

Šepić, J., Vilibić, I., & Monserrat, S. (2016). Quantifying the probability of meteotsunami occurrence from synoptic atmospheric patterns. *Geophysical Research Letters*, *43*(19), 10,377-10,384. https://doi.org/10.1002/2016GL070754

Šepić, J., Vilibić, I., Rabinovich, A., & Tinti, S. (2018). Meteotsunami ("Marrobbio") of 25–26 June 2014 on the Southwestern Coast of Sicily, Italy. *Pure and Applied Geophysics*, *175*(4), 1573–1593. https://doi.org/10.1007/s00024-018-1827-8

Shi, L., Olabarrieta, M., Valle-Levinson, A., & Warner, J. C. (2019). Relevance of wind stress and wave-dependent ocean surface roughness on the generation of winter meteotsunamis in the Northern Gulf of Mexico. *Ocean Modelling*, *140*(December 2018), 101408. https://doi.org/10.1016/j.ocemod.2019.101408

Shiga, T., Ichikawa, M., Kusumoto, K., & Suzuki, H. (2007). *A statistical study on seiche around Kyushu and Satsunan Islands*. *Papers in Meteorology and Geophysics* (Vol. 74).

Song, Y. T., Fukumori, I., Shum, C. K., & Yi, Y. (2012). Merging tsunamis of the 2011 Tohoku-Oki earthquake detected over the open ocean. *Geophysical Research Letters*, *39*(5). https://doi.org/10.1029/2011GL050767

Tanaka, K. (2010). Atmospheric pressure-wave bands around a cold front resulted in a meteotsunami in the East China Sea in February 2009. *Natural Hazards and Earth System Science*, *10*(12), 2599–2610. https://doi.org/10.5194/nhess-10-2599-2010

Thomson, R. E., Rabinovich, A. B., Fine, I. V., Sinnott, D. C., McCarthy, A., Sutherland, N. A. S., & Neil, L. K. (2009). Meteorological tsunamis on the coasts

of British Columbia and Washington. *Physics and Chemistry of the Earth*, *34*(17–18), 971–988. https://doi.org/10.1016/j.pce.2009.10.003

Tolkova, E., Nicolsky, D., & Wang, D. (2017). A Response Function Approach for Rapid Far-Field Tsunami Forecasting. *Pure and Applied Geophysics*, *174*(8), 3249–3273. https://doi.org/10.1007/s00024-017-1612-0

Torrence, C., & Compo, G. P. (1998). A Practical Guide to Wavelet Analysis. *Bulletin of the American Meteorological Society*, *79*(1), 61–78. https://doi.org/10.1175/1520-0477(1998)079<0061:APGTWA>2.0.CO;2

Tsushima, H., Hino, R., Fujimoto, H., Tanioka, Y., & Imamura, F. (2009). Near-field tsunami forecasting from cabled ocean bottom pressure data. *Journal of Geophysical Research*, *114*(B6), B06309. https://doi.org/10.1029/2008JB005988

Tsushima, H., Hino, R., Tanioka, Y., Imamura, F., & Fujimoto, H. (2012). Tsunami waveform inversion incorporating permanent seafloor deformation and its application to tsunami forecasting. *Journal of Geophysical Research: Solid Earth*, *117*(B3), 1–20. https://doi.org/10.1029/2011JB008877

Uematsu, A., Nakamura, R., Nakajima, Y., & Yajima, Y. (2013). X-band interferometric SAR sensor for the Japanese altimetry mission, COMPIRA. In *2013 IEEE International Geoscience and Remote Sensing Symposium - IGARSS* (pp. 2943–2946). IEEE. https://doi.org/10.1109/IGARSS.2013.6723442

Vilibić, I. (2008). Numerical simulations of the Proudman resonance. *Continental Shelf Research*, *28*(4–5), 574–581. https://doi.org/10.1016/j.csr.2007.11.005

Vilibić, I., Domijan, N., Orlić, M., Leder, N., & Pasarić, M. (2006). Resonant couppling of a traveling air pressure disturbance with the east Adriatic coastal waters. *Annales Geophysicae*, *24*(11), 2759–2771. https://doi.org/10.1029/2004JC002279

Vilibić, I., Monserrat, S., Rabinovich, A., & Mihanović, H. (2008). Numerical modelling of the destructive meteotsunami of 15 June, 2006 on the coast of the Balearic Islands. *Pure and Applied Geophysics*, *165*(11–12), 2169–2195. https://doi.org/10.1007/s00024-008-0426-5

Vilibić, I., Šepić, J., Ranguelov, B., Mahović, N. S., & Tinti, S. (2010). Possible atmospheric origin of the 7 May 2007 western Black Sea shelf tsunami event. *Journal of Geophysical Research*, *115*, 1–12. https://doi.org/10.1029/2009JC005904

Vilibić, I., Šepić, J., Rabinovich, A. B., & Monserrat, S. (2016). Modern Approaches in Meteotsunami Research and Early Warning. *Frontiers in Marine Science*, *3*(May), 1–7. https://doi.org/10.3389/fmars.2016.00057

Webb, D. J. (2013). On the shelf resonances of the English Channel and Irish Sea. *Ocean Science*, *9*(4), 731–744. https://doi.org/10.5194/os-9-731-2013

Wertman, C. a, Yablonsky, R. M., Shen, Y., Merrill, J., Kincaid, C. R., & Pockalny, R. a. (2014). Mesoscale convective system surface pressure anomalies responsible for meteotsunamis along the U.S. East Coast on June 13th, 2013. *Scientific Reports*, *4*, 7143. https://doi.org/10.1038/srep07143

Williams, D. A., Horsburgh, K. J., Schultz, D. M., & Hughes, C. W. (2019). Examination of Generation Mechanisms for an English Channel Meteotsunami: Combining Observations and Modeling. *Journal of Physical Oceanography*, *49*(1), 103–120. https://doi.org/10.1175/JPO-D-18-0161.1

Yanuma, T., & Tsuji, Y. (1998). Observation of Edge Waves Trapped on the Continental Shelf in the Vicinity of Makurazaki Harbor, Kyushu, Japan. *Journal of Oceanography*, *54*(1), 9–18. Retrieved from

https://link.springer.com/article/10.1007/BF02744377